Title: SALICYLIC ACID SENSOR1 reveals the propagation of an SA hormone surge during plant pathogen advance

Authors: Bijun Tang[1], Jing Lu[1], Hana Leontovyčová[2], Gesa Hoffmann[3], James H. Rowe[1,4], Sacha Fouquay O'Donnell[1], Mathieu Grangé-Guermente[1], Bo Larsen[1], Rinukshi Wimalasekera[1]‡, Philip Carella[5], Marco Incarbone[3], Tetiana Kalachova[2], Alexander M. Jones[1]*

Affiliations:

[1]Sainsbury Laboratory, University of Cambridge; Cambridge, United Kingdom.

[2]Institute of Experimental Botany of the Czech Academy of Science; Prague, Czech Republic.

[3]Max Planck Institute of Molecular Plant Physiology; Potsdam, Germany.

[4]Plants, Photosynthesis and Soil, School of Biosciences, University of Sheffield; Sheffield, United Kingdom.

[5]Cell and Developmental Biology, John Innes Centre; Norwich, United Kingdom.

‡Present address: Department of Botany, University of Sri Jayewardenepura; Nugegoda, Sri Lanka.

*Corresponding author: Alexander M. Jones. alexander.jones@slcu.cam.ac.uk

Abstract:
Salicylic acid (SA) is a key phytohormone that orchestrates immune responses against pathogens, including *Pseudomonas syringae* bacteria. The timing and extent of SA accumulation is tightly controlled by plants but can be supressed by pathogens to overcome immunity. Understanding SA dynamics at high spatiotemporal resolution remains challenging due to limitations in existing detection methods that are indirect, destructive, or lacking in cellular precision and temporal resolution. We developed SalicS1, a genetically-encoded FRET biosensor specific to SA. SalicS1 enables real-time, reversible monitoring of SA levels in vivo with minimal perturbation of endogenous signalling. We reveal the propagation of an SA surge spreading from bacterial infection sites with spatiotemporal fidelity. SalicS1 unlocks precise understanding of SA dynamics underpinning crop resilience to pathogens.

Main Text:

Introduction

Salicylic acid (SA) is a phytohormone that is critical for plant defences but is also involved in regulating physiological processes during development and responses to abiotic stress (*1–3*). Used widely as a topical medicine and as the feedstock for commercial acetylsalicylate (Aspirin) production, SA is an indispensable component of the plant immune system, acting to promote resistance induced by the pattern-triggered immunity (PTI) and effector-triggered immunity (ETI) pathways (1, 4, 5). In compatible interactions where plant immunity fails to prevent disease, for example *Pseudomonas syringe* pv *tomato* DC3000 (*Pst* DC3000) infection of *Arabidopsis thaliana*, SA accumulation slows bacterial growth and pathogenesis but does not ultimately prevent infection. By comparison, incompatible interactions generally promote high levels of SA that are associated with resistance. SA and its methylated form are also central to the systemic acquired resistance (SAR) response that confers broad-spectrum pathogen protection across plant organs (*6–9*).

SA biosynthesis in plants is mediated by two pathways named from chorismate utilising enzymes ISOCHORISMATE SYNTHASE (ICS) and PHENYLALANINE AMMONIA-LYASE (PAL), with the ICS pathway being dominant in Arabidopsis (*10*, *11*). Key regulators include AtICS1, the transporter ENHANCED DISEASE SUSCEPTIBILITY 5 (AtEDS5), the avrPphB SUSCEPTIBLE 3 (AtPBS3) enzyme (*11–15*), and transcriptional regulators like SAR DEFICIENT 1 (SARD1) and CALMODULIN BINDING PROTEIN 60g (CBP60g) (*16*) that control ICS1, EDS5 and PBS3 induction. SA accumulation triggers transcriptional networks via NONEXPRESSOR OF PATHOGENESIS-RELATED GENES (NPR) receptors. NPR1, also known as NON-INDUCIBLE IMMUNITY (NIM1), is the central regulator of SA signaling that translocates to the nucleus upon SA binding and interacts with TGACG-binding TGA transcription factors to reprogram transcription and strengthen immune responses (*17–19*). Further modulation of SA signalling occurs through protein-protein interactions among NPR proteins (*17*), NPR1 post-translational modifications (*20*, *21*), and NPR1 interaction with NIM1-INTERACTING (NIMIN) proteins, adding additional layers of complexity to SA regulation. Pathogens have also evolved strategies to inhibit SA-mediated immunity, including directly lowering SA levels via the *nahG* encoded salicylate hydroxylase catabolic enzyme (*22*, *23*). Despite significant advancements in understanding the molecular pathways governing SA biosynthesis, modification and catabolism, SA dynamics across cells and subcellular compartments during infection – a crucial battleground in the evolutionary arms race between plant and pathogen – remain unknown.

Traditional SA detection methods such as high-performance liquid chromatography (HPLC) (*24*, *25*) provide quantitative information but are destructive and lack the spatial and temporal resolution needed to track SA dynamics at the cellular level. Indirect methods, including *PATHOGENESIS-RELATED PROTEIN 1 (PR1) promoter*-based reporters (*26*), improve spatiotemporal resolution but provide only semi-quantitative data on SA activity and are sensitive to non-SA regulated signalling event. Bacteria engineered to respond to SA with luminescence reporters can be deployed to apolplasmic spaces, but cannot report intracellular SA levels or temporal dynamics (27). Electrochemical and nanotube-based SA sensing technologies have shown promise for use in vivo and do not require transgenic plants, but require creation and application of devices or chemical probes and lack specificity for bioactive SA (*28*, *29*). Protein-based Fluorescence Resonance Energy Transfer (FRET)-biosensors that co-opt sensory domains

adapted to ligand perception, once expressed in the organism of interest, uniquely offer the combination of minimally-invasive, specific, quantitative and spatially resolved analyte detection over time (*30*, *31*).

To address the need for real-time, high-resolution monitoring of SA, we developed SALICYLIC ACID SENSOR1 (SalicS1), a genetically-encoded Fluorescence Resonance Energy Transfer (FRET)-based biosensor specific for SA. SalicS1 enables direct, reversible detection of SA within the Arabidopsis physiological range, providing a precise tool for tracking SA dynamics in response to biotic stresses. SalicS1 revealed accumulation of micromolar levels of exogenous SA in yeast and in Arabidopsis root nuclei as well as biologically relevant induction of endogenous SA in nuclei of Arabidopsis leaves under bacterial, fungal and insect attack.

Results

Engineering SalicS1 with an accelerated FRET-based biosensor screening platform

FRET biosensors for the hormones Abscisic Acid and Gibberellin, ABAleon, ABACUS and GPS, co-opted hormone-induced protein-protein interactions into sensory modules by sandwiching two-part hormone binding domains between fluorescent proteins (FP) of a FRET pair (*32–36*). In the latter biosensors, ligand binding promotes an intramolecular interaction that increases the energy transfer between the donor and acceptor FPs, which is quantified by measuring a positive change in fluorescence emission ratio after excitation of the donor (*33*, *36*). We envisioned SalicS1 as a negative ratio change sensor designed to co-opt the SA-induced disruption of NPR-NIMIN protein interactions previously discovered in yeast-2-hybrid assays of *Nicotiana tabacum* proteins (**Fig. 1A, fig. S1)** (*37*, *38*).

We initially screened biosensor designs using high-affinity AtNPR3 (*17*) fused with AtNIMIN1 as the sensory domain using a two-part combinatorial Gateway-based engineering platform previously used to develop several FRET biosensors (*33*, *34*, *39–41*). Sensor candidates were expressed in protease-deficient yeast (*42*) and screened in whole cells or lysates. A slight emission ratio change was observed using AtNPR3-AtNIMIN in combination with several FRET pairs when analysed in whole cells (**fig. S2A, table S1**). However, analysis of yeast cell lysates showed loss of FRET while maintaining fluorescence, indicating cleavage of the sensory domain (**fig. S2B**). Based on NtNPR1 and NtNIMIN interaction studies (*38*), we reasoned that retaining only the SA-binding C-terminus of NPR1 may stabilize the protein, avoid post-translational modifications (*21*, *43*) (**fig. S1C**), and retain SA-sensitive NIMIN interaction while reducing interaction with other endogenous components (*44*) (**fig. S1D,E**). Together these changes would result in a more orthogonalized biosensor with reduced likelihood of causing phenotypes (*36*, *45*) or being sensitive to non-specific signalling events when expressed in planta. Truncated AtNPR1t and NtNPR1t linked with AtNIMIN1 and NtNIMIN1-L, respectively, were screened in both orientations with a series of FRET pairs (**table S1, fig. S2C**). The NPR1 truncations successfully enabled screening of SA-induced emission ratio change in yeast cell lysates and NtNPR1t and NtNIMIN1-L were selected as sensory domains for further optimisation.

We next established an accelerated five-part combinatorial Golden Gate-based platform (**Fig. 1B, table S2**) to improve the FRET biosensor screening process (**fig. S1B**). Modelled after our Gateway platform, Golden-gate modules encoding for NtNPR1t-NtNIMIN1-L, NtNPR1t-

NtNIMIN1-L linkers (X-linkers) of different lengths and flexibilities were synthesized (**table S3**). The linker between FP and sensory domains is an important target for optimizing FRET biosensor signal-to-noise ratio (*46*) and a series of FRET pair FPs was also generated (**table S2**). A total of 62 variant combinations were screened in yeast cell lysates (**fig. S2D, table S4**). The optimized SalicS1 biosensor consists of an N-terminal edAFPt9 (enhanced dimer Aphrodite with 9 aa C-terminal truncation) linked via a Serine-Proline linker to NtNPR1t, connected by L52 to NtNIMIN1-L, and finally linked via a Proline-Leucine linker to edCerulean (**Fig. 1C**). AlphaFold predicted that in the absence of SA, alpha-helix 3 of NtNPR1t would interact with an alpha-helix of NtNIMIN1-L (**fig. S1E**). Upon SA binding, we predicted the interaction between NtNPR1t and NtNIMIN1-L would be disrupted, causing an opening of the sensory domain that reduces FRET and lowers the emission ratio (**Fig. 1D**).

Engineering of SalicS1 variants

A series of non-responsive (NR) and low-affinity (LA) SalicS1 variant candidates were designed based on mutation of highly conserved or possible SA binding NtNPR1t residues from previous structural analysis of AtNPR4 (*47*) (**fig. S3A-C**). High-affinity (HA) candidates were designed based on mutation of NtNPR1t residues to corresponding residues in high affinity AtNPR3 and AtNPR4 (*17*) (**fig. S3A,C**). The dissociation constants (K_d^{SA}) and dynamic range of 21 variants were determined for purified biosensors *in vitro* (**table S5, fig. S3D**). The final selected variants—SalicS1, SalicS1-NR (R431Q), SalicS1-HA (K424R), and SalicS1-LA (F508A)—had K_d^{SA} values of 8.1 µM, N/A, 1.6 µM, and 36.0 µM, respectively (**Fig. 1E**). In a specificity test against SA derivatives, precursors and metabolites, purified SalicS1 responded specifically to SA (**fig. S4A**), while SalicS1-HA also responded to acetylsalicylate with lower emission ratio change than for SA (**Fig. 1F, fig. S4A,B**). SalicS1 was also determined to be rapidly reversible suggesting it could report both accumulation and depletion of SA (**Fig. 1G, fig. S4C**).

In planta validation of SalicS

Stable transgenic *Arabidopsis* lines were generated using the constitutive p16 promoter (*48*) and Tnos terminator. An N-terminal nuclear-localisation sequence (nls) was fused to SalicS1 and variants to facilitate image analysis of nuclear patterns across neighboring cells and to measure SA levels in a highly relevant subcellular compartment. Expression of nlsSalicS1 did not cause detectable phenotypic changes in roots or rosette leaves compared to Wildtype (WT) Col-0 (**Fig. 1H,I**).

When imaged in roots, hypocotyls, cotyledons, and mature leaves, nlsSalicS1 indicated cellular SA levels in living plants, though basal SA levels might fall near or below nlsSalicS1 detection range (see below, **Fig. 2A, fig. S5A**). A predicted reduction in nlsSalicS1 and -HA and -LA variant but not -NR variant emission ratio was observed with exogenous 10 µM SA treatments in roots, cotyledons, and mature leaves (**Fig. 2B-E, fig. S5B-C, fig. S6A-C**). Similar to in vitro experiments, nlsSalicS1 biosensor responses were dose-dependent in planta with response to sub-micromolar exogenous SA (**fig. S6D**) and reversible with ability to detected repeat treatment after a buffer wash (**fig S6E**). Based on highest expression level in T2 seedlings and maximum SA response (SalicS1, -HA and –LA) or minimum non-response (NR) in planta, transgenic lines were selected for further experiments (**fig. S7A,B**). Taken together, these results suggested that nlsSalicS1 was not saturated for SA detection in the organs studied, confirmed the ability of plant cells to accumulate and deplete exogenous SA and indicated that nlsSalicS1-NR can serve as a negative control for detection of non-specific biosensor responses.

A gradient of biosensor emission ratio was observed in roots expressing both nlsSalicS1 and -NR variants, indicating artifact arising from non-SA mediated biosensor dynamics (e.g. interaction between NtNIMIN1-L and endogenous components such as NPR1, NPR3 or NPR4 proteins). To exclude the possibility that SA-induced emission ratio changes of nlsSalicS1 in vivo results from interaction with endogenous NPR proteins and not SA binding, we generated *npr* mutant lines (*npr1-1* and *npr3-2, npr4-3* double mutant (46)), expressing nlsSalicS1. The pattern of SA distribution and emission ratio change upon exogenous SA application was similar in WT and mutants, indicating nlsSalicS1 response is not dependent on endogenous NPR proteins (**Fig. 2F, fig. S8A**).

To further validate the sensor, nlsSalicS1 lines overexpressing the *nahG* (*22*) SA catabolic enzyme (nlsSalicS1-pUBQ10::NahG) were generated (**fig. S8B**). Before SA treatment, nlsSalicS1 emission ratios were comparable between WT and NahG overexpression lines, possibly indicating low basal SA levels in roots (**Fig. 2G,H, fig. S5D**). As anticipated, NahG overexpression prevented both biosensor responses to exogenous SA as well as exogenous SA accumulation as detected by an SA-responsive bacterial bioassay (*50*), (**Fig. 2G,H, fig. S8C**). Additionally, *eds5-1* and *pbs3* biosynthesis mutants expressing nlsSalicS1 also showed comparable SA levels to untreated WT, consistent with low basal SA levels in roots and mature leaves being at or below the detection range of nlsSalicS1 in the cell types analysed (**fig. S9A-C**). As expected, these mutants were still responsive to exogenous SA (**fig. S9A-C**). In both NahG overexpression and the biosynthetic mutants, the gradient of emission ratio is again observed in roots before and after exogenous SA, suggesting an artifact that is unrelated to SA levels as observed in nlsSalicS1-NR lines.

To check whether expression of nlsSalicS1 could affect immunity negatively, whether by overepression of the tobacco NIMIN1-L moiety or via buffering of SA, we tested bacterial growth and SA content measured with bacterial bioassay (*47*) in WT Col-0, nlsSalicS1, PR1::GUS, PR1::Venus and NahG overexpression lines. In both assays, NahG but not nlsSalicS1 overexpression resulted in decreased immunity (**fig. S10**). To assess the relative sensitivity of in vivo SA detection by SalicS1 vs destructive SA quantification by bacterial bioassay (*47*), we compared seedlings exposed to 0.5 µM and 1 µM exogenous SA and found nlsSalicS1 was more sensitive to sub-micromolar levels (**fig. S10 C,D**).

Validation of nlsSalicS1 dynamics under biotic stress

Using nlsSalicS1, we observed SA induction in Arabidopsis in response to diverse biotic invaders, including the bacterium *Pst* DC3000, the non-adapted fungus *Blumeria graminis pv hordei* (*Bgh*) and the specialized aphid *Brevicoryne brassicae (B. brassicae)* (**Fig. 3A, fig. S11A-E**) at varying concentrations after 1 or 2 days post infection. *Pst* infiltration ensured relatively homogenous colonisation of the leaf, and significant increases in bioassay quantified SA levels (*50*) (**Fig. 3B**) alongside downstream signalling induction detected by pPR1-GUS and pPR1-Venus reporter lines (*51*, *52*). The fungus *Bgh* is not adapted to Arabidopsis, so SA increased locally where spores germinated but failed to invade epidermal cells, producing patchy responses across the leaf that were detectable by SalicS1 and other reporters in the groups of cells surrounding the infected cell (**fig. S12A-C**). *B. brassicae* aphids preferentially inject stylets into the veins (*53*), and while SA induction or responses were not detected through destructive quantification in total leaf extracts, SA responses were detected in the cells directly surrounding the puncture site by pPR1::GUS and pPR1::Venus reporters. Overall, these results with semi-quantitative SA signalling reporters were

comparable to SA accumulation quantified by nlsSalicS1 (**Fig. 3A**). In the case of *B. brassicae*, only SalicS1 and pPR1-GUS were sensitive enough to detect significant increases in SA.

nlsSalicS1 reveals the propagation of SA surge during pathogen advance

To interrogate local responses to infection, we introduced bacteria into Arabidopsis by piercing a single area of the leaf with a fine-point needle carrying *Pst* DC3000. In response to the localised application of *Pst* DC3000, we observed strong SA accumulation at the inoculation site at 20 hrs, but also broad SA accumulation, which even crossed the midvein (**Fig. 3C, fig. S13A**). A detailed cellular analysis of nlsSalicS1 vs nlsSalicS1-NR revealed that both epidermal and stomatal cells accumulate SA where no significant change of SA accumulation is reported by nlsSalicS1-NR (**fig. S14**). As anticipated, reduced SA induction was observed in both the *eds5* mutant and *pUBQ10::Nah*G plants, with *pUBQ10::NahG* showing lower basal SA levels compared to WT and *eds5* leaves (**Fig. 3D,E, fig. S13B**). nlsSalicS1-NR does not respond to *Pst* DC3000 with lowered emission ratios (**Fig. 3D,E, fig. S13B**).

Using in planta nlsSalicS1, we detected differences in SA induction in WT *Pst* DC3000 and a series of mutants with altered immune induction, for example infection with the polyeffector mutant D36E (*51*) or the type III secretion system mutant *hrpA*- (*52*) did not lead to significant SA induction at 20 hrs after needle inoculation (**Fig. 4A,B, fig. S15A**). In comparison, two avirulent *Pst* DC3000 strains (i.e. avrRpm1 and avrRpt2) expected to induce high levels of SA following activation of ETI, showed high but spatially restricted SA induction at 20 hrs (**Fig. 4A,B, fig. S15A**). The distribution of SA accumulation differed between ETI-activating avrRpm1 or avrRpt2 carrying *Pst* DC3000 relative to the WT control, with avirulent strains inducing SA accumulation nearer to the infection site, while the WT strain promoted a more widespread distribution (**Fig. 4C, fig. S16A**). Thus, nlsSalicS1 revealed both absolute and spatial differences in SA accumulation during interactions with immune activating or disease-promoting *Pst* strains. Taken together, these results validate nlsSalicS1 for minimally-invasive, high-resolution quantification of SA levels in vivo. Time series analysis revealed SA induction around 14 to 17 hours after infection in response to local application with *Pst* DC3000 (**Fig. 4D, E, fig. S15B**). SA levels are thought to quantitatively affect the outcome of infection, ranging from full resistance to susceptibility, yet the specific relationship between SA level and bacterial spread remains unclear. Key questions include whether high local SA concentration limit pathogen spread or if *Pst* DC3000 actively reduces SA levels in infected regions. To begin to explore these questions, we used *Pst* DC3000 expressing mCherry to track bacterial dissemination relative to SA distribution visualized by the nlsSalicS1 biosensor. *Pst* DC3000-mCherry and WT *Pst* DC3000 induced similar levels of SA and red fluorescence was only detected in *Pst* DC3000-mCherry infections (**fig. S16B,C**). We used mCherry fluorescence to categorize Arabidopsis cell nuclei into groups that are proximal or distal to bacterial infection sites. Proximal cells more directly exposed to bacteria exhibited higher SA levels from 11-20 hours, whereas distal cells were slower and accumulated SA after 17 hours post infection (**Fig. 4F,G, fig. S15C**). A time-series showed the cellular basis of a surge of SA spreading from the *Pst* inoculation site (**Fig. 4H, fig. S15D, Movie. S1, fig. S16D**). Furthermore, during a 7-day systemic infection with Turnip mosaic virus expressing 6K2:Scarlet, SA levels increased in WT but not *pUBQ10::NahG* leaves with invading virus (**fig. S17A,B**).

Discussion

Pathogens suppress plant immune responses to proliferate within host tissues, while plants use SA as a critical defence signal to limit infection. High-resolution detection of SA-related immune

events during *Pst* DC3000 infection such as NPR1 condensate formation (*54*) and single-cell RNA sequencing of defence associated gene expression (*55*) have revealed the localised nature of plant immunity. However, the nucleus-by-nucleus nature of SA dynamics determining the balance between infection and immunity remained unclear. When expressed in Arabidopsis nuclei, nlsSalicS1 revealed high-resolution SA dynamics in living organs in a minimally-invasive manner.

While previous studies demonstrate that ETI inducing strains of *Pst* DC3000 provoke higher SA levels than WT (*56*), whole leaf infiltrations and bulk SA quantification fail to account for the spatial organisation of immunity. For example, spatially restricted Arabidopsis infection assays with *Pst* carrying avrRpt2 demonstrated *PR1* gene expression only in cell layers immediately surrounding infection sites (*57*), which is broadly consistent with our direct visualisation of SA accumulation using SalicS1. The SA antagonist jasmonic acid is likely responsible for tightly constraining SA signalling, as it similarly accumulates to high levels (*58*,*59*) and the JA marker *VSP1* encircles *PR1*-responding cells during ETI responses associated with immune-related cell death (5*7*). A precise mapping of the quantitative relationship between cellular SA accumulation, PR1 gene activation and JA marker gene activation during localised ETI awaits further study. Such future research leveraging spatially aware technologies like SalicS1 can reveal how plants control SA to promote a robust local immune response while also maintaining cell survival in adjacent cells and tissues.

Tracking nlsSalicS1 emission ratios in combination with mCherry-expressing *Pst* DC3000 during infection, we found that a surge of SA accumulation begins at proximal cells exposed to bacteria and extends outwards to distal cells over time. This distal SA accumulation adds defense hormone context to the discovery of distinct immune transcriptomes in multiple leaf cell populations during *Pst* DC3000 infection (*55*). It remains to be determined whether this SA surge results from local synthesis in distal cells or translocation of the SA hormone itself, though the progression over hours suggests SA depletion mechanisms are sufficient to limit simple diffusive spread (*56*). It will also be important to decipher how broad-based SA accumulation quantitatively impacts not only pathogen spread and systemic acquired resistance induction, but also stomatal aperture and plant growth, which are also regulated by SA (*60*, *61*). Future biosensor engineering efforts could also further optimise SalicS1 to detect higher concentrations of SA or to reveal the source of and avoid the root gradient artifact of the present biosensors. Furthermore, as a transferable genetically encoded part (*62*, *63*), the SalicS1 FRET biosensor has the potential to be adapted for use in additional subcellular compartments (e.g. with chloroplast transit peptides), diverse taxa (e.g. aspirin fluxes in human cells) as well as in crop plants where SA is a conserved determinant of disease and immunity.

References:

1. R. F. White, Acetylsalicylic acid (aspirin) induces resistance to tobacco mosaic virus in tobacco. *Virology* **99**, 410–412 (1979).
2. I. Raskin, Salicylate, A New Plant Hormone. *Plant Physiol* **99**, 799–803 (1992).
3. S. H. Spoel, X. Dong, Salicylic acid in plant immunity and beyond. *Plant Cell* **36**, 1451–1464 (2024).
4. C. Zipfel, Plant pattern-recognition receptors. *Trends in Immunol* **35**, 345-351 (2014).
5. J. Malamy, J. P. Carr, D. F. Klessig, I. Raskin, Salicylic Acid: a likely endogenous signal in the resistance response of tobacco to viral infection. *Science* **250**, 1002–1004 (1990).
6. J. P. Métraux, H. Signer, J. Ryals, E. Ward, M. Wyss-Benz, J. Gaudin, K. Raschdorf, E. Schmid, W. Blum, B. Inverardi, Increase in salicylic acid at the onset of systemic acquired resistance in cucumber. *Science* **250**, 1004–1006 (1990).
7. W. E. Durrant, X. Dong, Systemic acquired resistance. *Annu Rev Phytopathol* **42**, 185–209 (2004).
8. C. An, Z. Mou, Salicylic Acid and its function in plant immunity. *J Integr Plant Biol* **53**, 412-428 (2011).
9. J. D. G. Jones, R. E. Vance, J. L. Dangl, Intracellular innate immune surveillance devices in plants and animals. *Science* **354**, aaf6395 (2016).
10. C. Nawrath, J.-P. Métraux, Salicylic acid induction-deficient mutants of arabidopsis express PR-2 and PR-5 and accumulate high levels of camalexin after pathogen inoculation. *The Plant Cell* **11**, 1393-1404 (1999).
11. H. Lefevere, L. Bauters, G. Gheysen, Salicylic Acid biosynthesis in plants. *Front in Plant Sci* **11**, 338 (2020).
12. M. C. Wildermuth, J. Dewdney, G. Wu, F. M. Ausubel, Isochorismate synthase is required to synthesize salicylic acid for plant defence. *Nature* **414**, 562-565 (2001).
13. D. Rekhter, D. Lüdke, Y. Ding, K. Feussner, K. Zienkiewicz, V. Lipka, M. Wiermer, Y. Zhang, I. Feussner, Isochorismate-derived biosynthesis of the plant stress hormone salicylic acid. *Science* **365**, 498-502 (2019).
14. C. Nawrath, S. Heck, N. Parinthawong, J. P. Métraux, EDS5, an essential component of salicylic acid-dependent signaling for disease resistance in Arabidopsis, is a member of the MATE transporter family. *Plant Cell* **14**, 275–286 (2002).
15. M. P. Torrens-Spence, A. Bobokalonova, V. Carballo, C. M. Glinkerman, T. Pluskal, A. Shen, J. K. Weng, PBS3 and EPS1 Complete Salicylic Acid Biosynthesis from Isochorismate in Arabidopsis. *Mol Plant* **12**, 1577–1586 (2019).
16. L. Wang, K. Tsuda, W. Truman, M. Sato, L. V. Nguyen, F. Katagiri, J. Glazebrook, CBP60g and SARD1 play partially redundant critical roles in salicylic acid signaling. *Plant Journal* **67**, 1029–1041 (2011).
17. Y. Ding, T. Sun, K. Ao, Y. Peng, Y. Zhang, X. Li, Y. Zhang, Opposite Roles of Salicylic Acid Receptors NPR1 and NPR3/NPR4 in Transcriptional Regulation of Plant Immunity. *Cell* **173**, 1454-1467.e10 (2018).
18. W. Fan, X. Dong, In Vivo interaction between NPR1 and transcription factor TGA2 leads to salicylic acid-mediated gene activation in arabidopsis. *Plant Cell* **14**, 1377–1389 (2002).
19. A. Rochon, P. Boyle, T. Wignes, P. R. Fobert, C. Després, The coactivator function of Arabidopsis NPR1 requires the core of its BTB/POZ domain and the oxidation of C-terminal cysteines. *Plant Cell* **18**, 3670–3685 (2006).

20. Y. Tada, S. H. Spoel, K. Pajerowska-Mukhtar, Z. Mou, J. Song, C. Wang, J. Zuo, X. Dong, Plant immunity requires conformational charges of NPR1 via S-nitrosylation and thioredoxins. *Science* **321**, 952–956 (2008).
21. A. Saleh, J. Withers, R. Mohan, J. Marqués, Y. Gu, S. Yan, R. Zavaliev, M. Nomoto, Y. Tada, X. Dong, Posttranslational modifications of the master transcriptional regulator NPR1 enable dynamic but tight control of plant immune responses. *Cell Host Microbe* **18**, 169–182 (2015).
22. L Friedrich, B Vernooij, T Gaffney, Characterization of tobacco plants expressing a bacterial salicylate hydroxylase gene. *Plant Mol. Bio.* **29**, 959-968 (1995).
23. T. P. Delaney, S. Uknes, B. Vernooij, L. Friedrich, K. Weymann, D. Negrotto, T. Gaffney, M. Gut-Rella, H. Kessmann, E. Ward, J. Ryals, A central role of salicylic acid in plant disease resistance. *Science* **266**, 1247-1250 (1994).
24. I. Raskin, I. M. Turnert, W. R. Melander, Regulation of heat production in the inflorescences of an Arum lily by endogenous salicylic acid. *Proc.Natl.Acad.Sci.U.S.A.* **86**, 3324-2218 (1989).
25. G. Marek, R. Carver, Y. Ding, D. Sathyanarayan, X. Zhang, Z. Mou, A high-throughput method for isolation of salicylic acid metabolic mutants. *Plant Methods* **6**, 21 (2010).
26. T. Pečenková, R. Pleskot, V. Žárský, Subcellular localization of Arabidopsis pathogenesis-related 1 (PR1) protein. *Int J Mol Sci* **18**, 825 (2017).
27. W. E. Huang, L. Huang, G. M. Preston, M. Naylor, J. P. Carr, Y. Li, A. C. Singer, A. S. Whiteley, H. Wang, Quantitative in situ assay of salicylic acid in tobacco leaves using a genetically modified biosensor strain of Acinetobacter sp. ADP1. *Plant J.* **46**, 1073–1083 (2006).
28. A. H. Bukhamsin, S. S. Shetty, E. Fakeih, M. S. Martinez, C. Lerma, M. Mundummal, J. Y. Wang, J. Kosel, S. Al-Babili, I. Blilou, K. N. Salama, In vivo dynamics of indole- and phenol-derived plant hormones: Long-term, continuous, and minimally invasive phytohormone sensor. *Sci. Adv.* **11**, eads8733 (2025).
29. M. C. Y. Ang, J. M. Saju, T. K. Porter, S. Mohaideen, S. Sarangapani, D. T. Khong, S. Wang, J. Cui, S. I. Loh, G. P. Singh, N. H. Chua, M. S. Strano, R. Sarojam, Decoding early stress signaling waves in living plants using nanosensor multiplexing. *Nat Commun* **15**, 2943 (2024).
30. A. Miyawaki, J. Llopis, R. Heim, J. M. Mccaffery, J. A. Adams, M. Ikurak, R. Y. Tsien, "Fluorescent indicators for Ca 2+ based on green fluorescent proteins and calmodulin" *Nature* **388**, 882-887 (1997).
31. J. H. Rowe, M. Josse, B. Tang, A. M. Jones, Quantifying plant biology with fluorescent biosensors. Annu Rev Plant Biol **76**, 285–315 (2025).
32. R. Waadt, K. Hitomi, N. Nishimura, C. Hitomi, S. R. Adams, E. D. Getzoff, J. I. Schroeder, FRET-based reporters for the direct visualization of abscisic acid concentration changes and distribution in Arabidopsis. *Elife,* **3**, e01739 (2014).
33. A. M. Jones, J. Å. Danielson, S. N. ManojKumar, V. Lanquar, G. Grossmann, W. B. Frommer, Abscisic acid dynamics in roots detected with genetically encoded FRET sensors. *Elife* **3**, e01741 (2014).
34. A. Rizza, A. Walia, V. Lanquar, W. B. Frommer, A. M. Jones, In vivo gibberellin gradients visualized in rapidly elongating tissues. *Nat. Plants* **3**, 803-813 (2017).
35. A. Rizza, B. Tang, C. E. Stanley, G. Grossmann, M. R. Owen, L. R. Band, A. M. Jones, Differential biosynthesis and cellular permeability explain longitudinal gibberellin gradients in growing roots. *Proc.Natl.Acad.Sci.U.S.A* **118**, e19211960118 (2021).

36. J. H. Rowe, M. Grangé-Guermente, M. Exposito-Rodriguez, R. Wimalasekera, M. Lenz, K. Shetty, S. R. Cutler, A. M. Jones, Next-generation ABACUS biosensors reveal cellular ABA dynamics driving root growth at low aerial humidity. *Nat. Plants* **9**, 1103-1115 (2023).
37. R. R. Weigel, C. Bäuscher, A. J. P. Pfitzner, U. M. Pfitzner, NIMIN-1, NIMIN-2 and NIMIN-3, members of a novel family of proteins from Arabidopsis that interact with NPR1/NIM1, a key regulator of systemic acquired resistance in plants. *Plant Mol. Biol.* **46**, 143-160 (2001).
38. M. Hermann, F. Maier, A. Masroor, S. Hirth, A. J. P. Pfitzner, U. M. Pfitzner, The Arabidopsis NIMIN proteins affect NPR1 differentially. *Front. Plant. Sci.* **4**, 88 (2013).
39. C. H. Ho, W. B. Frommer, Fluorescent sensors for activity and regulation of the nitrate transceptor CHL1/NRT1.1 and oligopeptide transporters. *Elife* **3**, e01917 (2014).
40. C. L. Cuevas-Velazquez, T. Vellosillo, K. Guadalupe, H. B. Schmidt, F. Yu, D. Moses, J. A. N. Brophy, D. Cosio-Acosta, A. Das, L. Wang, A. M. Jones, A. A. Covarrubias, S. Sukenik, J. R. Dinneny, Intrinsically disordered protein biosensor tracks the physical-chemical effects of osmotic stress on cells. *Nat Commun* **12**, 5438 (2021).
41. Y.-N. Chen, H. N. Cartwright, C.-H. Ho, In vivo visualization of nitrate dynamics using a genetically encoded fluorescent biosensor. *Sci Adv.* **8**, eabq4915 (2022).
42. E. W. Jones, Tackling the protease problem in Saccharomyces cerevisiae. *Methods Enzymol* **194**, 428–453 (1991).
43. S. H. Spoel, Z. Mou, Y. Tada, N. W. Spivey, P. Genschik, X. Dong, Proteasome-mediated turnover of the transcription coactivator NPR1 plays dual roles in regulating plant immunity. *Cell* **137**, 860–872 (2009).
44. S. Kumar, R. Zavaliev, Q. Wu, Y. Zhou, J. Cheng, L. Dillard, J. Powers, J. Withers, J. Zhao, Z. Guan, M. J. Borgnia, A. Bartesaghi, X. Dong, P. Zhou, Structural basis of NPR1 in activating plant immunity. *Nature* **605**, 561–566 (2022).
45. J. Griffiths, A. Rizza, B. Tang, W. B. Frommer, A. M. Jones, GIBBERELLIN PERCEPTION SENSOR 2 reveals genesis and role of cellular GA dynamics in light-regulated hypocotyl growth. *Plant Cell* **36**, 4426-4441 (2024).
46. M. Balcerowicz, K. N. Shetty, A. M. Jones, Fluorescent biosensors illuminating plant hormone research. *Plant Physiol* **187**, 590–602 (2021).
47. W. Wang, J. Withers, H. Li, P. J. Zwack, D. V. Rusnac, H. Shi, L. Liu, S. Yan, T. R. Hinds, M. Guttman, X. Dong, N. Zheng, Structural basis of salicylic acid perception by Arabidopsis NPR proteins. *Nature* **586**, 311–316 (2020).
48. C. Schuster, C. Gaillochet, A. Medzihradszky, W. Busch, G. Daum, M. Krebs, A. Kehle, J. U. Lohmann, A regulatory framework for shoot stem cell control integrating metabolic, transcriptional, and phytohormone signals. *Dev. Cell* **28**, 438–449 (2014).
49. Z. Q. Fu, S. Yan, A. Saleh, W. Wang, J. Ruble, N. Oka, R. Mohan, S. H. Spoel, Y. Tada, N. Zheng, X. Dong, NPR3 and NPR4 are receptors for the immune signal salicylic acid in plants. *Nature* **486**, 228–232 (2012).
50. C. T. Defraia, E. A. Schmelz, Z. Mou, A rapid biosensor-based method for quantification of free and glucose-conjugated salicylic acid. *Plant Methods* **4**, 28 (2008).
51. A. D. Shapiro, C. Zhang, The role of NDR1 in avirulence gene-directed signaling and control of programmed cell death in Arabidopsis. *Plant Physiol.* **127**, 1089–1101 (2001).
52. Lorenzo Poncini, Ines Wyrsch, Vale´rie De´nervaud Tendon, Thomas Vorley, Thomas Boller, Niko Geldner, Jean-Pierre Me´traux, Silke Lehmann, In roots of Arabidopsis thaliana, the damage- associated molecular pattern AtPep1 is a stronger elicitor of immune signalling than flg22 or the chitin heptamer. *PLoS One* **12**, e0185808 (2017).

53. N. Rubil, T. Kalachova, T. P. Hauser, L. Burketová, Specialist aphid feeding causes local activation of salicylic and jasmonic acid signaling in Arabidopsis veins. *Mol. Plant-Microbe Interact.* **35**, 119–124 (2022).
54. R. Zavaliev, R. Mohan, T. Chen, X. Dong, Formation of NPR1 condensates promotes cell survival during the plant immune response. *Cell* **182**, 1093-1108.e18 (2020).
55. T. Nobori, A. Monell, T. A. Lee, J. Zhou, J. Nery, J. R. Ecker, Time-resolved single-cell and spatial gene regulatory atlas of plants under pathogen attack. bioRxiv Preprint (2023). doi: https://www.biorxiv.org/content/10.1101/2023.04.10.536170v2
56. J. L. Carviel, D. C. Wilson, M. Isaacs, P. Carella, V. Catana, B. Golding, E. A. Weretilnyk, R. K. Cameron, Investigation of intercellular salicylic acid accumulation during compatible and incompatible Arabidopsis-Pseudomonas syringae interactions using a fast neutron-generated mutant allele of EDS5 identified by genetic mapping and whole-genome sequencing. *PLoS One* **9**, e88608 (2014).
57. S. Betsuyaku, S. Katou, Y. Takebayashi, H. Sakakibara, N. Nomura, H. Fukuda, Salicylic acid and jasmonic acid pathways are activated in spatially different domains around the infection site during effector-triggered immunity in Arabidopsis thaliana. *Plant Cell Physiol* **59**, 8–16 (2018).
58. L. Liu, F. M. Sonbol, B. Huot, Y. Gu, J. Withers, M. Mwimba, J. Yao, S. Y. He, X. Dong, Salicylic acid receptors activate jasmonic acid signalling through a non-canonical pathway to promote effector-triggered immunity. *Nat Commun* **7**, 13099 (2016).
59. S. H. Spoel , A. Koornneef , S. M. Claessens, J. P. Korzelius, J. A. Van Pelt, M. J. Mueller, A. J. Buchala, J. P. Métraux, R. Brown, K. Kazan, L. C. Van Loon, X. Dong, C. M. Pieterse, NPR1 modulates cross-talk between salicylate- and jasmonate-dependent defense pathways through a novel function in the cytosol. *Plant Cell* **15**, 760–770 (2003).
60. M. Rivas-San Vicente, J. Plasencia, Salicylic acid beyond defence: Its role in plant growth and development. *J Exp Bot* **62**, 3321-3338 (2011).
61. L. Xu, H. Zhao, J. Wang, X. Wang, X. Jia, L. Wang, Z. Xu, R. Li, K. Jiang, Z. Chen, J. Luo, X. Xie, K. Yi, AIM1-dependent high basal salicylic acid accumulation modulates stomatal aperture in rice. *New Phytol.* **238**, 1420–1430 (2023).
62. C. Drapek, A. Rizza, N. A. Mohd-Radzman, K. Schiessl, F. Dos Santos Barbosa, J. Wen, G. E. D. Oldroyd, A. M. Jones, Gibberellin dynamics governing nodulation revealed using GIBBERELLIN PERCEPTION SENSOR 2 in Medicago truncatula lateral organs. *Plant Cell* **36**, 4442-4456 (2024).
63. S. Zhang, D. A. Daniels, S. Ivanov, L. Jurgensen, L. M. Müller, W. K. Versaw, M. J. Harrison, A genetically encoded biosensor reveals spatiotemporal variation in cellular phosphate content in Brachypodium distachyon mycorrhizal roots. *New Phytol.* **234**, 1817–1831 (2022).
64. B, Tang, (2025). Raw data for SALICYLIC ACID SENSORS1 reveals the propogation of an SA hormone surge during pathogen advance. https://doi.org/10.17863/CAM.119273.
65. J.H. Rowe. (2025). FRETENATOR Analysis Toolset. https://doi.org/10.5281/zenodo.16843696
66. C. Engler, R. Kandzia, S. Marillonnet, A one pot, one step, precision cloning method with high throughput capability. *PLoS One* **3**, e3647 (2008).
67. E. Weber, C. Engler, R. Gruetzner, S. Werner, S. Marillonnet, A modular cloning system for standardized assembly of multigene constructs. *PLoS One* **6**, e16765 (2011).
68. J. Abramson, J. Adler, J. Dunger, R. Evans, T. Green, A. Pritzel, O. Ronneberger, L. Willmore, A. J. Ballard, J. Bambrick, S. W. Bodenstein, D. A. Evans, C. C. Hung, M. O'Neill, D. Reiman, K. Tunyasuvunakool, Z. Wu, A. Žemgulytė, E. Arvaniti, C. Beattie,

O. Bertolli, A. Bridgland, A. Cherepanov, M. Congreve, A. I. Cowen-Rivers, A. Cowie, M. Figurnov, F. B. Fuchs, H. Gladman, R. Jain, Y. A. Khan, C. M. R. Low, K. Perlin, A. Potapenko, P. Savy, S. Singh, A. Stecula, A. Thillaisundaram, C. Tong, S. Yakneen, E. D. Zhong, M. Zielinski, A. Žídek, V. Bapst, P. Kohli, M. Jaderberg, D. Hassabis, J. M. Jumper, Accurate structure prediction of biomolecular interactions with AlphaFold 3. *Nature* **630**, 493–500 (2024).

69. LLC. Schrödinger, The PyMOL Molecular Graphics System, Version 3.0 Schrödinger, LLC. *The PyMOL Molecular Graphics System, Version3.0* (2024).
70. R. De Michele, C. Ast, D. Loqué, C. H. Ho, S. L. A. Andrade, V. Lanquar, G. Grossmann, S. Gehne, M. U. Kumke, W. B. Frommer, Fluorescent sensors reporting the activity of ammonium transceptors in live cells. *Elife* **18**, e06986 (2013).
71. S. Nagaya, K. Kawamura, A. Shinmyo, K. Kato, The HSP terminator of arabidopsis thaliana increases gene expression in plant cells. *Plant Cell Physiol* **51**, 328–332 (2010).
72. P. Marhavý, A. Kurenda, S. Siddique, V. Dénervaud Tendon, F. Zhou, J. Holbein, M. S. Hasan, F. M. Grundler, E. E. Farmer, N. Geldner, Single-cell damage elicits regional, nematode-restricting ethylene responses in roots. *EMBO J* **38**, e100972 (2019).
73. H. Cao, J. Glazebrook, J. D. Clarke, The Arabidopsis NPR1 Gene That Controls Systemic Acquired Resistance Encodes a Novel Protein Containing Ankyrin Repeats. *Cell* **88**, 57-63 (1997).
74. Y. Zhang, Y. T. Cheng, N. Qu, Q. Zhao, D. Bi, X. Li, Negative regulation of defense responses in Arabidopsis by two NPR1 paralogs. *Plant J.* **48**, 647–656 (2006).
75. S. J. Clough, A. F. Bent, Floral dip: A simplified method for Agrobacterium-mediated transformation of Arabidopsis thaliana. *Plant J.* **16**, 735–743 (1998).
76. B. E. Lindsey, L. Rivero, C. S. Calhoun, E. Grotewold, J. Brkljacic, Standardized method for high-throughput sterilization of Arabidopsis seeds. *J.Vis.Exp* **17**, 56587 (2017). doi: 10.3791/56587.
77. J. Schindelin, I. Arganda-Carreras, E. Frise, V. Kaynig, M. Longair, T. Pietzsch, S. Preibisch, C. Rueden, S. Saalfeld, B. Schmid, J. Y. Tinevez, D. J. White, V. Hartenstein, K. Eliceiri, P. Tomancak, A. Cardona, Fiji: An open-source platform for biological-image analysis. *Nat. Methods **9**, 676-682* (2012).
78. K. J. Livak, T. D. Schmittgen, Analysis of relative gene expression data using real-time quantitative PCR and the 2-ΔΔCT method. *Methods* **25**, 402–408 (2001).
79. T. Kalachova, M. Janda, V. Šašek, J. Ortmannová, P. Nováková, I. Petre Dobrev, V. Kravets, A. Guivarc'h, D. Moura, L. Burketová, O. Valentová, E. Ruelland, Identification of salicylic acid-independent responses in an Arabidopsis phosphatidylinositol 4-kinase beta double mutant. *Ann Bot* **125**, 775–784 (2020).
80. M. Incarbone, G. Bradamante, F. Pruckner, T. Wegscheider, W. Rozhon, V. Nguyen, R. Gutzat, Z. Mérai, T. Lendl, S. MacFarlane, M. Nodine, & O.M. Scheid, Salicylic acid and RNA interference mediate antiviral immunity of plant stem cells, Proc. Natl. Acad. Sci. U.S.A. 120 (42) e2302069120, https://doi.org/10.1073/pnas.2302069120 (2023).
81. R. A. Jefferson, T. A. Kavanagh', M. W. Bevan, GUS fusions: beta-glucuronidase as a sensitive and versatile gene fusion marker in higher plants. *EMOB J* **6**, 3901-3907 (1987).
82. Z. Krčková, D. Kocourková, M. Daněk, J. Brouzdová, P. Pejchar, M. Janda, I. Pokotylo, P. G. Ott, O. Valentová, J. Martinec, The Arabidopsis thaliana non-specific phospholipase C2 is involved in the response to Pseudomonas syringae attack. *Ann Bot* **121**, 297–310 (2018).
83. A. Rizza, A. Walia, B. Tang, A. M. Jones, Visualizing cellular gibberellin levels using the nlsGPS1 förster resonance energy transfer (FRET) biosensor. *J. Vis. Exp* (2019). doi: 10.3791/58739.

84. J. H. Rowe, A. Rizza, A. M. Jones, Quantifying phytohormones in vivo with FRET biosensors and the FRETENATOR analysis toolset. *Environmental Responses in Plants: Methods and Protocols* **2494**, 239-253 (2022).

5

Acknowledgments: We thank Mary C. Wildermuth for kindly providing *eds5* and *pbs3* seeds used in this study and Sebastian Schornack and Ankit Walia for helpful comments on the manuscript. We thank all staff of the SLCU for lab support, horticulture support and especially to Ray Wightman and Gareth Evans from Core Microscopy Unit for supporting the Confocal imaging experiments. H.L. and T.K. acknowledge IEB Imaging Facility and support by project of Ministry of Education, Youth and Sports "National Infrastructure for Biological and Medical Imaging (Czech-BioImaging – LM2023050)". This work was supported by the Gatsby Charitable Foundation (GAT3395) and European Research Council (H2020-EU.1.1. - EXCELLENT SCIENCE - European Research Council (ERC) agreement no. 759282) to A.M.J.

Funding:

Gatsby Charitable Foundation (GAT3395) (AMJ)

European Research Council (H2020-EU.1.1. - EXCELLENT SCIENCE - European Research Council (ERC) agreement no. 759282) (AMJ)

Czech-BioImaging – LM2023050 (TK)

Author contributions:

Conceptualization: BT, AMJ

Methodology: BT, JL, HL, GH, SO, MG, BL, RW, PC, TK, MI

Visualization: BT, TK, AMJ

Funding acquisition: TK, AMJ

Supervision: AMJ

Writing – original draft: BT, AMJ

Writing – review & editing: BT, JL, JR, PC, TK, AMJ

Competing interests: Authors declare that they have no competing interests.

Data and materials availability: Arabidopsis transgenic lines with nlsSalicsS1, nlsSalicS1-NR and nlsSalicS1-pUBQ10::NahG are deposited to Nottingham Arabidopsis Stock Centre (NASC IDs N2112676, N2112677, N2112678). Plasmids with nlsSalicsS1 and nlsSalicS1-NR are deposited to Addgene (Plasmids 232190, 232192). All other transgenic plant lines and plasmids are available upon request. All data in this manuscript are available at the Cambridge data repository (doi.org/10.17863/CAM.119273) (*64*). Code is available at https://doi.org/10.5281/zenodo.16843696 (*65*).

Supplementary Materials:

Materials and Methods

Figs. S1 to S17

Tables S1 to S6

References (*66–84*)

Movie S1

Data S1 to S2

Figure Legends:

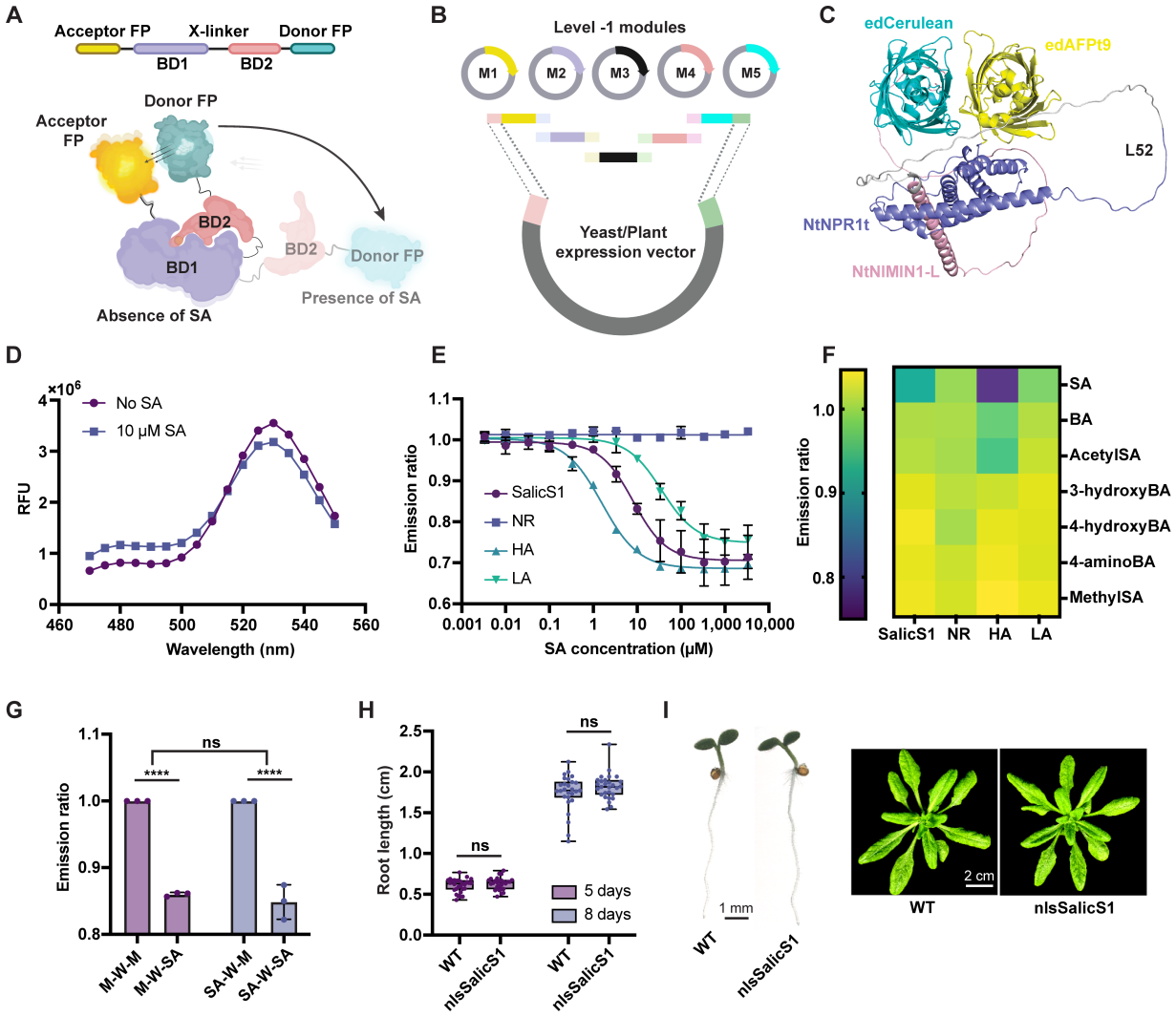

Fig. 1. Design and engineer SalicS1 and their variants. (**A**) SalicS1 is a negative ratio change sensor consisting of four main domains, Binding Domain 1,2 (BD1,2), Fluorescence Proteins 1,2 (FP1,2) and three key linkers. In the absence of SA, there are more FRET between the donor FP and the acceptor FP, whereas in the presence of SA, the conformational change of the sensory domain resulting less FRET, therefore lower emission ratio. (**B**) Golden Gate-based screening platform was built for FRET-based sensor screening in a high throughput manner. The platform consists of five main modules which are donor and acceptor FP, two components of the sensory domain and the X-linker. (**C**) AlphaFold3 predicted structure for SalicS1. *Predicted local distance difference test confidence score*: 0.61 (**D**) Emission spectrum of the determined SalicS1 with and without SA (n=5). RFU: Relative Fluorescence Unit. (**E**) Dose response curve of SalicS1, -NR, -HA and -LA with K_d^{SA} value 8.1 μM, N/A, 1.6 μM and 36.0 μM from one representative experiment (n=3). Experiments were independently performed three times. (**F**) Specificity test of SalicS1 and its variants to 10 μM of SA and structurally related chemicals from one representative experiment (n=3). The experiment was independently performed three times. (**G**) Reversibility test for SalicS1. Error bars represent SD. M: Mock, W: Wash, SA: 10 μM SA (n=3). One representative experiment was analysed with *Two-way ANOVA, uncorrected Fisher's LSD, ****P value* <

0.0001, ns = non-significant. Experiments were independently performed two times. (**H**) Phenotyping experiment for 5 and 8-days-old seedlings of Arabidopsis (WT vs nlsSalicS1, n=29,27,27,28). One representative experiment was analysed with *Two-way ANOVA, Uncorrected Fisher's LSD, ns = non-significant.* Root length comparison between Col-0 WT and nlsSalicS1 at 5 days and 8 days show no significant difference between. Each point indicates the length of an individual root. For boxplots, centre line indicates median; box limits indicate upper and lower quartiles; whiskers indicate the upper/lower adjacent values. (**I**) **Left:** Representative images of 5-days-old seedling stages between Col-0 WT vs nlsSalicS1. **Right**: Representative images of 4-weeks-old rosette stages between Col-0 WT vs nlsSalicS1 (n=15). Experiments were independently performed three times. (**G&H**) Exact P-values for all comparison, F values and degress of freedom were provided in **Data S1**.

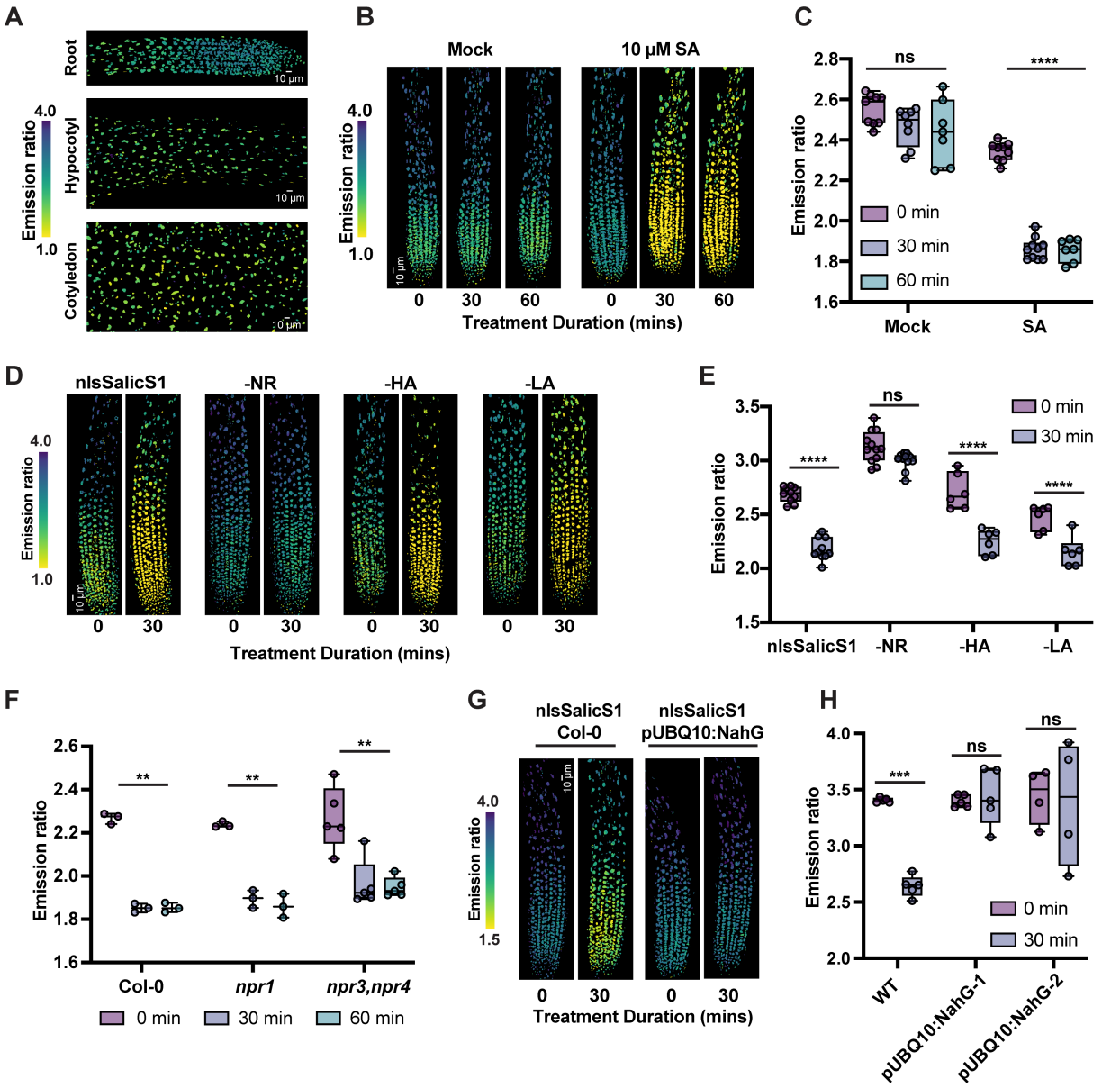

Fig. 2. In planta validation for nlsSalicS1 in stably transformed Arabidopsis. (**A**) Endogenous pattern of SA reported by nlsSalicS1 in 5 days old seedlings at root, hypocotyl and cotyledon (LUT: 1.0-4.0, n=10). (**B**) nlsSalicS1 reported increased SA after exogenous 10 µM SA application. False coloured Images of roots before and after mock or 10 µM SA treatment (LUT: 1.0-4.0). (**C**) Significant reduction of emission ratio is observed in the treatment group whereas no significant difference was observed in the mock treatment group. Each dot represents the average of all nucleuses in one sample (n=9,8,7,9,10,7). *Repeated measures Two-way ANOVA, Sidak's multiple comparisons test, ****P value < 0.0001, ns = non-significant P value > 0.05*. The sample size for individual data points was 440-820 nuclei in an image of 581.82 x 145.45 µm. (**D**) Representative images of nlsSalicS1, -HA, -LA and -NR reported different levels of emission ratio change when 10 µM exogenous SA was applied (LUT: 1.0-4.0). (**E**) Significant difference in emission ratio after 10 µM of SA application were observed in nlsSalicS, -HA and -LA whereas no significant difference was reported in -NR (n=10,10,12,10,6,6,6,6). *Repeated measures Two-way ANOVA, Sidak's multiple comparisons test, **** <0.0001, ns = non-significant P value >*

0.05. The sample size for individual data points was 360-940 nuclei in an image of 581.82 x 145.45 µm. (**F**) Significant differences were reported by nlsSalicS1 in Col-0 WT, *npr1* mutant and *npr3 npr4* double mutants (n=3,3,5). *Repeated measures Two-way ANOVA, Tukey's multiple comparisons test, **P value < 0.01*. The sample size for individual data points was 530-1100 nuclei in an image of 581.82 x 145.45 µm. (**G**) Representative images of nlsSalicS1 when 10 µM SA was applied to pUBQ10::NahG (overexpressed NahG) mutant (LUT:1.5-4.0). (**H**) Quantification of emission ratio of nlsSalicS1 in WT Col-0 vs pUBQ10::NahG (n=5,5,4). *Repeated measures Two-way ANOVA, Sidak's multiple comparisons test, ***P value = 0.0002, ns = non-significant P value > 0.05*. The sample size for individual data points was 360-560 nuclei in an image of 581.82 x 145.45 µm. (**B-H**): Experiments repeated three times independently. Each point indicates the mean nuclear emission ratio for an individual root z-stack. For boxplots, centre line indicates median; box limits indicate upper and lower quartiles; whiskers indicate the upper/lower adjacent values. Analysis test was performed on one representative repeat and exact P value, F value, degree of freedom are provided in **Data S1**.

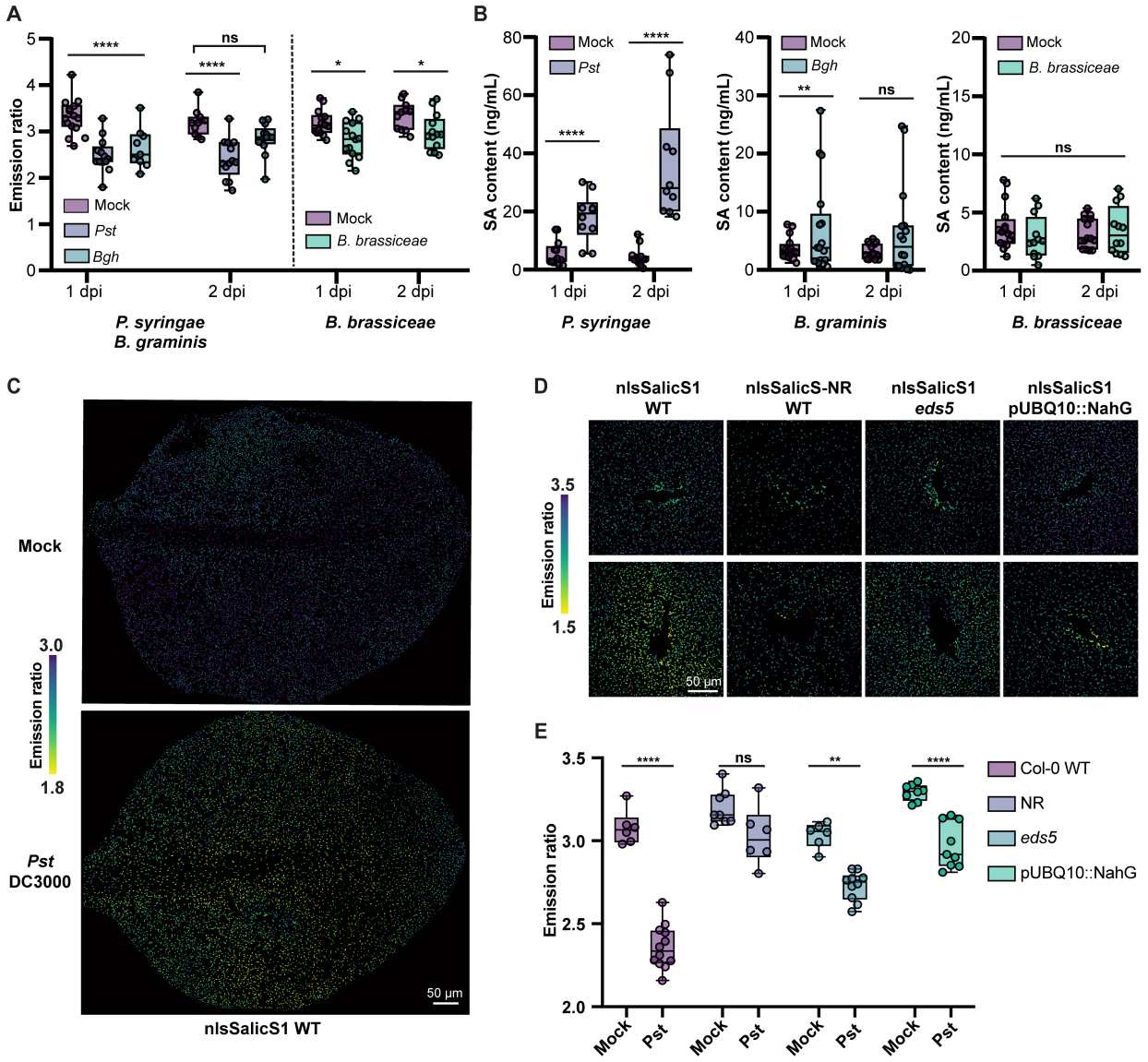

Fig. 3. nlsSalicS1 reported SA accumulation under biotic stress. (**A**) Emission ratio reported by nlsSalicS1 upon *P. syringae pv tomato* DC3000 *(Pst)*, *B. graminis (Bgh)* and *B. brassiceae (Bb)* infection 1 and 2 days post infection (dpi). *Two-way ANOVA with Sidak's multiple comparisons test, ****P value < 0.0001,* *P value were provided in **Data S1**; *ns = non-significant in all comparisons, P value > 0.05*. Mock (n=14,11), *Pst* (n=13), *Bgh* (n=9), *Bb* infested (n=14,11). The sample size for individual data points was 1500-2800 nuclei in an image of 1553.04 x 1553.04 µm. (**B**) SA quantification by *Acinetobacter* sp. *ADPWH_lux* luminescence upon infection 1 and 2 dpi. *Two-way ANOVA with Sidak's multiple comparisons test, ****P value < 0.0001, **P value < 0.01; ns = non-significant in all comparisons*, *P value > 0.05*. Mock (n=13,14), *Pst* (n=10), *Bgh* (n=6,16), *Bb* infested (n=12,12). (**C**) Represented images of 3 weeks old nlsSalicS1mature leave under mock vs *Pst* DC3000 infection 20 hours after infection (n=3, LUT: 1.8-3.0). (**D**) Representative images for nlsSalicS1 WT Col-0 (n=6), nlsSalicS-NR WT Col-0 (n=6), nlsSalicS1 *eds5* (n=6) and nlsSalicS1 pUBQ10::NahG (n=8) upon mock (Upper) vs *Pst* DC3000 (Lower) inoculation 20 hrs post infection (hpi). LUT: 1.5-3.5. (**E**) Quantification of emission ratio of nlsSalicS1 in different background after mock vs *Pst* DC3000 infection. *Two-way ANOVA with*

*Sidak multiple comparisons test, ****P value < 0.0001, **P value = 0.0027, ns = non-significant P value > 0.05*. The sample size for individual data points was 1100-2800 nuclei in an image of 1553.04 x 1553.04 µm. Analysis was performed on one represented experiment. Experiments were repeated two times independently. Each point indicates the mean nuclear emission ratio for an individual root z-stack. For boxplots, centre line indicates median; box limits indicate upper and lower quartiles; whiskers indicate the upper/lower adjacent values. Exact P value, F value, degree of freedom are provided in **Data S1**.

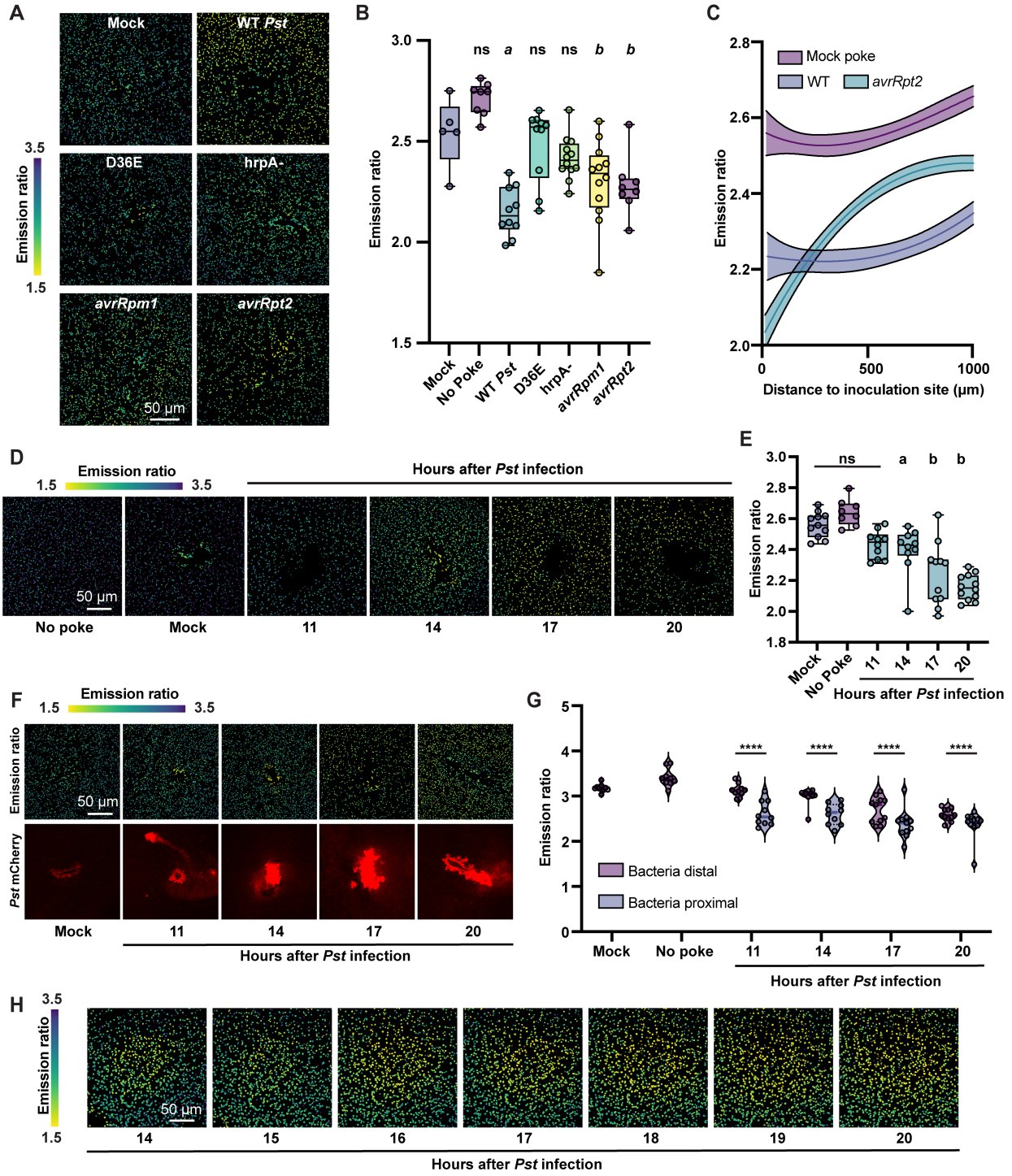

Fig. 4. nlsSalicS1 reported SA in high spatiotemporal manner under *Pst* DC3000 infection. (**A**) Representative images of nlsSalicS1 reported different emission ratio changes upon different *Pst* DC3000 mutant strains infection 20 hrs after infection. No poke (n=8), Mock poke (n=5), *Pst* DC3000 (n=9), D36E (n=8), *hrpA*- (n=9), *avrRpm1* (n=10), *avrRpt2* (n=10, LUT: 1.5-3.5). (**B**) Quantification of emission ratio under *Pst* mutants' infection. *One-way ANOVA analysis is performed against the mock control a: P value < 0.001, b: P value = 0.0172 (avrRpm1), P value = 0.0138 (avrRpt2)), ns = non-significant P value > 0.05.* (**C**) Emission ratio of nlsSalicS1 under mock poke, *Pst* DC3000 WT and *avrRpt2* variants treatment 20 hpi against the distance of nucleus

to inoculation site. Non-linear third order polynomial fit, shaded area represented confidence band = 95% (n=8). (**D**) Pseudo-time course of representative images for nlsSalicS1 in 3 weeks old mature leaves after infection. (**E**) Quantification of emission ratio under *Pst* DC3000 infection in pseudo-time course No poke: n=8, Mock: n=11, 11 hrs: n=10, 14 hrs: n-10, 17 hrs: n=11, 20 hrs: n=12. *One-way ANOVA, Dunnett's multiple comparisons test was performed against the mock control, a: P value = 0.0329, b: P value < 0.0001, ns = non-significant*. (**F**) Representative images reported by nlsSalicS1 vs *Pst* DC3000-mCherry in pseudo-time course (LUT: 1.5-3.5). (**G**) Significant difference reported between non-bacteria touching nucleus vs bacteria touching nucleus is reported during the pseudo-time course. *Two-way ANOVA, Tukey's multiple comparisons test, ****P value < 0.0001* (n=10). (**H**) nlsSalicS1 reported a surge of SA in Arabidopsis leaves spreading out from the infection site in a time course (n=3). After analysis, nuclei were dilated to allow easy visual discrimination at this magnification. LUT: 1.5-3.5. **(B,E,G):** The sample size for individual data points was 900-2900 nuclei in an image of 1553.04 x 1553.04 µm. **(A-F**): Analysis was performed on one representative experiment. Experiments were performed three times independently. Each point indicates the mean nuclear emission ratio for an individual root z-stack. For boxplots, centre line indicates median; box limits indicate upper and lower quartiles; whiskers indicate the upper/lower adjacent values. Exact P value, F value, degree of freedom are provided in **DataS1**.

Science
AAAS

Supplementary Materials for

SALICYLIC ACID SENSOR1 reveals the propagation of an SA hormone surge during pathogen advance

Bijun Tang[1], Jing Lu[1], Hana Leontovyčová[2], Gesa Hoffmann[3], James H. Rowe[1,4], Sacha Fouquay O'Donnell[1], Mathieu Grangé-Guermente[1], Bo Larsen[1], Rinukshi Wimalasekera[1]‡, Philip Carella[5], Marco Incarbone[3], Tetiana Kalachova[2], Alexander M. Jones[1]*

Corresponding author: alexander.jones@slcu.cam.ac.uk

The PDF file includes:

Other Supplementary Materials for this manuscript include the following:

Materials and Methods

Establishment of a combinatorial biosensor screening platform

A modular platform: Level -1 FRET-based biosensor screening platform for FRET biosensor development was established using Golden Gate cloning (*66*). The platform comprises five modules: **M1 (FP1)** - the donor fluorescent protein; **M2 (BD1)** - the first binding domain; **M3 (X-linker)** - a linker connecting BD1 and BD2; **M4 (BD2)** - the second binding domain; and **M5 (FP2)** - the acceptor fluorescent protein. This design, adapted from a Gateway cloning-based platform (*33*), enables more flexible assembly of FRET biosensors. Recognition sites (GAAGAC) for Type IIS restriction enzyme *BpiI* (Thermo Fisher Scientific) were incorporated into the vector flanking the coding regions, enabling the efficient insertion of modules into the Level 0 vectors that can express in yeast, bacteria or intermediate vector to go into plant expression vector. The overhang sequences flanking the coding regions, along with the antibiotic resistance markers used for cloning, are detailed in the Golden Gate library (**table S2**). The overhang design at M1 and M5 allows for the modular assembly of the sensor into the Golden Gate-Yeast expression vectors (gg-Yeast expression vector) generated using *EspIII* restriction enzymes (Thermo Fisher Scientific) (Ampicillin resistance gene for selection in bacteria and URA3 marker gene for selection in yeast), or an intermediate vector (EC41308, Enabling Nutrient Symbioses in Agriculture, ENSA) in the desired order. A Golden Gate scare of four nucleotide bases is left in the final cloning product due to overhang, and two extra nucleotides were added to create a two amino acids linker. Some of these linkers have been further engineered to optimize the FRET emission ratio.

Generation of Level -1 modulesle

To generate the Level -1 modules, the desired genes were either synthesized (Genewiz-Azenta) or cloned into the appropriate Level -1 modules using NEBuilder HiFi DNA Assembly (NEB) according to manufacturer instructions. Single-point mutations on Level -1 modules were introduced using the QuikChange II XL Site-Directed Mutagenesis Kit (Agilent) according to manufacturer instructions. A full list of Level -1 modules can be found in **table S2**. All primers used in this study are listed in **Data S2**.

Generation of SalicS candidates

Various combinations of five Level -1 modules were assembled into a Level 0 gg-Yeast expression vector to generate SalicS candidates for subsequent functional testing *in vitro*. The assembly was performed using a one-pot reaction involving *BpiI* (Thermo Fisher Scientific) restriction enzyme and T4 DNA ligase (NEB), following the Golden Gate reaction instructions (*67*).

Structure prediction and analysis

Protein structures, including SalicS1, linkers and sensory domains were predicted using AlphaFold3 (*68*). The amino acid sequences were prepared and input into the AlphaFold3 platform where default settings were used for multiple sequence alignment, template search and iterative model building. The predicted structure with high-confidence and better per-residue predicted local distance difference test (pLDDT) confidence score was used for structural assessment in

PyMOL (*69*). Distance between amino acids and molecule is measured by wizard measurement in PyMOL.

Sequence alignment

Sequences of different NPR proteins from various species were retrieved from The *Arabidopsis* Information Resource (TAIR) or Uniport, and Clustal Omega (Multiple Sequence Alignment MSA) was used for sequence alignment.

Generation of SalicS affinity series and non-responsive mutants

Single amino acid mutations within the NPR1 domain of SalicS1 in the BD1 Level -1 modules were generated using the QuikChange II XL Site-Directed Mutagenesis Kit (Agilent), following the manufacturers' instructions. All primers used for site-directed mutagenesis are listed in **Data S2**.

Expression of sensors in protease-deficient yeast

Saccharomyces cerevisiae strain BJ5465 (ATCC208289 *MATa ura3-52 trp1 leu2-Δ1 his3-Δ200 pep4:HIS3 prb1-Δ1.6 R* can*1 GAL*) (*33*) was transformed with Level 0 gg-Yeast expression plasmids with the desired candidate SalicS biosensors using lithium acetate transformation protocol (*70*). Yeast nitrogen base without amino acids (Sigma-Merck) and yeast synthetic drop-out medium supplements without uracil (Sigma-Merck) were used as transformers selective yeast media for complementation of uracil auxotrophy by the URA3 marker of the gg-yeast expression clone.

Preparation of yeast cells expressing biosensor protein candidates

Transformed yeast was grown in 5 ml cultures in SC medium-URA for two days. Yeast cell cultures were centrifuged at 4,000 g for 5 minutes. The cells were then transferred to 1.5 ml microcentrifuge tubes, resuspended in 20 mM MOPS (3-(N-morpholino) propane sulfonic acid) buffer (pH 7.4), and centrifuged again at 10,000 g for 1 minute. The cell pellets were resuspended in 20 mM MOPS buffer and transferred to 96-well flat-bottom clear microplates. A working solution of 100 µM SA was prepared from a 10 mM SA (Sigma-Aldrich) stock solution (dissolved in 99 % ethanol) diluted in 20 mM MOPS buffer. The working solution or mock treatment was added to 100 µl of the yeast cell suspension and incubated for 20 minutes before measured using SpectraMax i3x microplate reader (Molecular Devices).

Preparation of purified biosensor candidate proteins

Starting culture was set up as whole yeast cells yeast test then transferred to 100 ml SC -URA liquid culture for overnight at 30 ºC, 220 rpm. The cells were then transferred to 50 ml Falcon tubes and centrifuged at 4,000 g for 5 minutes and the supernatant was discarded. The cells were then resuspended in 20 mM MOPS, and centrifuged again at 4,000 g for 5 mins, and the supernatant was discarded. 1 ml of chilled silicon bead slurry (50 mM MOPS, pH 7.4, 0.1% Triton X-100, and 50 % v/v 0.5 mm zirconia/silica beads) was added to the yeast pellet in each tube. The

tubes were briefly vortexed to resuspend the cell pellets and then vortexed at maximum power at 4 ºC for 20 minutes. Following this, the tubes were centrifuged at 10,000 g at 4 ºC for 10 minutes. The supernatant was transferred to HisPur cobalt spin columns equilibrated with two resin-bed volumes of wash buffer (50 mM MOPS, 10 mM imidazole, 300 mM NaCl pH 7.4) (3 ml columns used in this project; Thermo Fisher Scientific). Prepared protein extract and resin were mixed on an end-over-end mixer for 30 minutes before centrifuge at 700 x *g* for 2 minutes and flow through was collected. Resin was then washed with two resin-bed volumes of wash buffer and centrifuged to collect flow through. His-tagged proteins were then collected with one resin-bed of elution buffer (50 mM MOPS, 500 mM imidazole, 300 mM NaCl, pH 7.4) by centrifuge at 700 x *g* for 2 minutes. The first elution from the purification column was diluted in 50 mM MOPS buffer (pH 7.4) and transferred to 96-well flat-bottom clear microplates (Greiner). A series of SA dilutions was prepared from a 10 mM stock solution in 99 % ethanol by serial dilution in 60 mM MOPS buffer (pH 7.4). A 50 µl volume of each SA dilution was added to 100 µl of sensor eluate followed by fluorescence analysis.

Fluorescence analysis of SA response

Fluorescence emission for CFP-YFP sensor candidates was recorded using a SpectraMax i3x microplate reader (Molecular Devices), scanning from 470–550 nm after excitation at 430 nm with a 5 nm bandwidth. The ratio was calculated by dividing the emission at 525–535 nm by the emission at 480–490 nm. For GFP-RFP candidates, the emission scan range was set for 495–625 nm with a step size of 5 nm and excitation at 485 nm. For BFP-GFP pairs, the emission scan range was set for 440–560 nm with a step size of 5 nm and excitation at 400 nm. For all imaging, the number of flashes was set to 10, and the integration time was set to 40 µs. Data were analyzed using Prism10 (GraphPad Software) to determine the dissociation constant (K_d^{SA}) and the ratio change for each candidate.

Specificity testing *in vitro*

SalicS1 and its variant proteins were purified using HisPur cobalt spin columns as previously described. Stock solutions (10 mM) of salicylic acid (Sigma-Aldrich), benzoic acid (Sigma-Aldrich), acetylsalicylic acid (Sigma-Aldrich), 3-hydroxybenzoic acid (Sigma-Aldrich), 4-hydroxybenzoic acid (Sigma-Aldrich), 4-aminobenzoic acid (Sigma-Aldrich), methyl salicylic acid (Sigma-Aldrich), and Salicylic acid 2-O-beta-D-glucoside (SAG, Santa Cruz Biotechnology) were prepared in ethanol. Working solutions of 10 µM for each compound were then prepared with 50 mM MOPS buffer (pH 7.4), and 50 µl of each working solution was added to the purified SalicS1 and its variants. Fluorescence emission was recorded using the SpectraMax i3x microplate reader, and data were analyzed as previously described.

Reversibility test *in vitro*

SalicS1 protein was purified using HisPur cobalt spin columns as previously described, treated with either wash buffer (20 mM MOPS, 300 mM NaCl, pH 7.4, containing 10 mM imidazole) or 100 µM salicylic acid (SA) diluted in the same buffer, then loaded onto Zeba™ spin desalting columns (Thermo Fisher Scientific) according to the manufacturer's instructions. One or two washes with wash buffer were performed prior to elution. The eluate was then transferred to a

second set of Zeba™ spin desalting columns, followed by additional washing and elution. After elution, the protein was treated with either wash buffer or 100 μM SA, and fluorescence emission was recorded using the SpectraMax i3x microplate reader. Data were analyzed as previously described.

Cloning SA catabolic enzyme constructs

DNA sequence coding for (*SALICYLATE HYDROXYLASE*) *NahG* was acquired from TAIR, codon optimized for *Arabidopsis thaliana*, synthesized (GENEWIZ-Azenta) and converted into Golden Gate module. *pUBQ10* from MoClo kit (*66*) was used to generate *pUBQ10::NahG* with Heat Shock terminator (tHSP) (*71*) Level 1 modules. The hygromycin resistance cassette and Promoter::*NahG*-Terminator were then incorporated into Golden Gate Level 2 Acceptors vector (pAGM4673, MoCloPlantToolKit).

Cloning SalicS1 and variants for expression in plants

The Golden Gate system was employed to generate SalicS1 and its variants for *in planta* expression. The following Level -1 modules were inserted into a Level 0 intermediate vector: 5' - a sequence coding for the SV40-derived nuclear localisation signal (LQPKKKRKVGG) and the enhanced dimer variant of Aphrodite with a nine-amino acid C-terminal truncation (edAFPt9); a sequence coding for the N-terminally truncated NtNPR1; a sequence coding for the L52 X-linker; a sequence coding for NtNIMIN1-L; a sequence coding for the enhanced dimer variant of Cerulean (edCer); and a sequence coding for the cMyc epitope tag -3'.

The *p16*, *pUBQ10*, and *p35S* promoters, along with the *tNOS* and *tHSP* terminators, were utilized to drive the expression of nuclear-localised SalicS1 and its variant biosensors in plants at Level 1. The Kanamycin resistance cassette and the Promoter::Sensor-Terminator construct were then inserted into Golden Gate Level 2 Acceptors vector (pAGM4673, MoCloPlantToolKit).

Plant material

WT, mutant, and transgenic lines seed in this study were Arabidopsis ecotype Columbia (Col-0). Transgenic lines of Arabidopsis in the Col-0 background used for microscopic observation were *PATHOGENESIS-RELATED PROTEIN 1* (*PR1*) promoter *pPR1::GUS* (*48*), *pPR1::NLS3xVenus* (*72*), *NahG* (*23*). SA signaling and biosynthesis mutants' lines expressing nlsSalicS1 were generated in this study from *npr1* (NASC: N3726) (*73*), *npr3-1 npr4-3* (NASC: N72352) (*74*), ENHANCED DISEASE SUSCEPTIBILITY 5 (*eds5*) and (AVRPPHB SUSCEPTIBLE 3 (*pbs3*). Catabolism overexpression mutants, *pUBQ10*::*NahG*:*tHSP* with nlsSalicS1 was generated in this study.

Plant transformation

The *Agrobacterium*-mediated floral dip method (*75*) was used to transform *Arabidopsis* Col-0, including the *npr3 npr4*, *eds5*, and *pbs3* mutant lines. Successful transformants were identified by kanamycin resistance selection on 1.2% agar (Duchefa Biochemie) plates containing ½ Murashige and Skoog (½ MS) basal medium (Duchefa Biochemi) with 0.025% (w/v) MES (Sigma, pH 5.7)

and 10 µM kanamycin. Fluorescence expression of transformants was analysed using a FluorChem Q imager (Alpha Innotech) with CY2 excitation and emission and the following settings: 12 second exposure time, normal speed, ultra-resolution and level 2 noise reduction.

Plant growth conditions

Seeds were surface sterilized using either chlorine gas treatment, 96 % ethanol (*76*) rinsed for 5 min followed by 100 % ethanol, or 30 % bleach solution with a droplet of Tween 20 for 5 minutes, rinsed 4 times with distilled water. Seeds were then sown on ½ MS medium with 0.025% MES (pH 5.7) in 0.8% agar plates or magenta vessel (Scientific Laboratory Supplies) for stratification at 4 ºC for 2 nights. For all imaging experiments, plants were grown under long-day conditions (110 µE, fluorescent light source, 22 ºC for 18 hours; 0 µE, 18 ºC for 6 hours, 70% relative humidity (RH) on plates or in magenta vessels excepts the plant material used for experiments shown in **Fig 3A & B**. These seeds were surface sterilized in a 30 % bleach solution (SAVO©, Unilever, Czech Republic) with a droplet of Tween 20 for 5 min, rinsed 4 times with distilled water and then stored for stratification at 4 °C for 2 nights. Subsequently, seeds were sown in Jiffy 7 peat pellets and plants were cultivated at 22 °C, 70 % relative humidity, under a short-day photoperiod (10 h light/14 h dark), at 100-130 µE m^{-2} s^{-1}. Plants were watered with distilled water and used for experiments when 4- to 5-weeks-old.

Phenotypic characterisation of plant lines expressing SalicS1

For root length assays, seeds were sown side by side in a vertical orientation on ½ MS medium with 0.025% MES (pH 5.7) in 0.8% agar plates and stratified at 4 ºC for 2 days. The plates were then transferred to a growth chamber under long-day conditions (110 µE, 22 ºC for 18 hours; 0 µE, 18 ºC for 6 hours). Images were captured 5 days and 8 days after the plates were transferred to light. Root lengths were measured using FIJI software (*77*). Homozygous biosensor-expressing lines were compared with isogenic wild-type lines segregated from heterozygous T1 parents.

RNA extraction and expression analysis

pUBQ10::NahG:tHSP overexpression seedlings were grown on ½ MS medium with 0.025% MES (pH 5.7) in 0.8% agar plates for 10 days under long-day conditions before harvest. Whole seedlings were collected for RNA extraction using the RNeasy Plant Mini Kit (Qiagen). Following DNase treatment (TURBO DNase, Invitrogen), 1 µg of total RNA was used for cDNA synthesis (SuperScript VILO cDNA Synthesis Kit, Invitrogen). Gene expression was quantified by RT-qPCR using LightCycler 480 SYBR Green I (Roche), with *PROTEIN PHOSPHATASE 2A SUBUNIT A3* (*PP2AA3*, Atg1g13320) as the internal control. Relative gene expression was analyzed using the 2^(-ΔCT) formula (*78*).

Adapted bacteria for infiltration assays

Pseudomonas syringae pv. *tomato* DC3000 (*Pst*) bacteria were cultivated overnight on plates containing LB medium (tryptone 10 g/L, NaCl 10 g/L, yeast extract 5 g/L, pH 7.0) supplemented with 1.4% agar and 50 mg/L rifampicin. Four-week-old plants (three leaves at similar developmental stage, i.e. 8^{th}-9^{th}-10^{th} mature true leaves) were syringe-infiltrated with the

suspension of *Pst* (OD_{600}=0.05 in 10 mM $MgCl_2$). At 1- and 2-days post inoculation, 3 discs (6 mm in diameter) were sampled from inoculated leaves from each plant, pooled (one plant as one sample) and homogenized in 1 ml of 10 mM $MgCl_2$, in a 2 ml Eppendorf tube, with 1 g of 1.3 mm silica beads using a FastPrep-24 instrument (MP Biomedicals, USA). The resulting homogenate was subjected to serial 10× dilutions and pipetted onto LB plates. Colonies were counted after 1–2 days of incubation at 26 °C. Six individual plants were used per treatment; bacterial load being expressed as $\log_{10}(CFU*mm^{-2})$ (*79*).

Bacteria for localised inoculation assays

Pseudomonas syringae pv. *tomato* DC3000 was used for WT *Pst* infection. In addition, *hrpA*-mutant (Rif and Kan resistance), D36E *polyeffector* mutant (Rif and Spec), *avrRpt2* (Rif and Kan) and *avrRpm1* (Rif and Kan) were used for the localised inoculation assay. Low salt LB agar (10 g/L bacto-tryptone, 5 g/L yeast extract 5 g/L NaCl, 20 g/L agar) was used for making the plate for growing *Pst* with appropriate antibiotic resistance. Plates are incubated at 28 ºC for two days before use. A fine needle (30Gx½, 0.3x13mm, TERUMO) was used to pick colonies on the plate and poke three mature true leaves (8^{th}-9^{th}-10^{th}) at similar developmental stage.

Non-adapted fungus

Blumeria graminis f. sp. *hordei* (*Bgh*) was cultivated continuously on winter barley (cv.Golden promise) grown under short day conditions (10 h /14 h light/dark) at 19 °C and 50% RH, at a light intensity of 70 µmol m^{-2} s^{-1}. *A. thaliana* plants were inoculated byspreading spores from infected barley onto the adaxial side (leaf to leaf) by compressed air pressure, 150–200 conidia per square mm (*79*).

Specialized herbivore

Cabbage aphid (*Brevicoryne brassicae*) was reared on 6-weeks-old broccoli or cabbage plants in an enclosed cage (45 x 45 x 45 cm) at 23 °C, photoperiod 16 h light/8 h dark. Plants were infested with 15 non-winged adult aphids (apterae), transferred on the leaves with a fine paint brush. Infested plants were kept individually in glass beakers covered with a fine mesh gauze, at 22 °C, 70 % RH, under 10 h light (100-130 µE m^{-2} s^{-1}) and 14 hours dark regime. Aphid-free plants served as controls and were kept under the same conditions. Aphids were removed from the leaves using the brush immediately before imaging or sample harvesting (*53*).

TuMV infection experiments

Seeds were surface-sterilized with ethanol and sown on ½ MS medium containing 1% sucrose and solidified with 0.8% agar. Following a 48-hour stratification period at 4 °C, seeds were germinated under long-day conditions (16 hours light at 50 µE from LED source, 22 °C; 8 hours at 0 µE, 22 °C). After 10 days, seedlings were transferred to Arabidopsis cultivation soil and grown for an additional 7 days under long-day conditions (16 hours light at 120 µE from LED source, 20 °C; 8 hours at 0 µE, 16 °C; 60% relative humidity). Plants were then rub-inoculated with TuMV-6K2:Scarlet (*80*). Imaging was performed on systemic symptomatic leaves at 7–8 days post-

infection, along with corresponding leaves from non-infected control plants. Infection was confirmed by detecting the viral 6K2:Scarlet protein using 561 nm laser wavelength.

Imaging of defence gene activation

The histochemical GUS assay (*81*) was performed on *pPR1*::GUS plants (*51*) as described previously (82). Briefly, leaves were submerged in X-GLUC (2 mM X-Gluc, 50 mM NaH_2PO_4, pH 7, 0.5 % (v/v) Triton-X, 0.5 mM K-ferricyanide) buffer for 16 hours at 37 °C; fixed and decolored in ethanol:glacial acetic acid (3:1 v/v), and further rehydrated in ethanol solutions, each applied for at least one hour in successive order: 70 % ethanol, 50 % ethanol and 30 % (v/v). Fully decolored leaves were then soaked in distilled water and left overnight in the dark. Leaves were scanned on Epson Perfection V700 Photo, at 1,000 dpi resolution.

To study the activation of expression of *pPR1::NLS3xVenus,* fluorescence was detected by fluorescence microscope Zeiss AxioImager ApoTome2 with EC Plan-Neofluar 5x/0.16 M27 objective and fluorescence cube FS09/GFP. The mean fluorescence intensity of the leaf discs (6 mm-diameter) was assessed by FIJI, 10 leaf discs (6 mm diameter) from three independent plants were used for one biological repetition. Cellular-resolution images of *pPR1::NLS3xVenus* were captured using Zeiss LSM 880 inverted confocal laser scanning microscope (Carl Zeiss AG, Germany), Plan-Apochromat 20x/0.8 DIC M27 objective, Ex=488 nm, detection 499–522 nm. Number of induced cells per ROI (400 μm^2) was quantified manually, at least 10 ROI from 3 independent plants per treatment were assessed.

Confocal imaging set up for FRET sensor imaging

An upright Leica SP8-Fliman, inverted Leica SP8-Iphox or upright Leica Stellaris 8 (Leica) confocal microscope was used for biosensor imaging in this study except for the experiments described in the previous session. Images were acquired as z-stacks in 12-bit mode, with a x10 or x20 dry 0.70 HCPLAN APO objective (Leica). Samples were mounted in ¼ MS (pH 5.7) for root imaging and leaf imaging. To excite the cyan fluorescent protein (CFP) variant, yellow fluorescent protein (YFP) variant, and mCherry, 448 nm, 514 nm and 552 nm lasers were used. Fluorescence emission was detected by HyD SMD detectors, set to detect 460 to 500 nm for CFP variant Cerulean, 525 to 560 nm for YFP variant Aphrodite and 590 to 635 nm for mCherry. The laser power was set between 5 % - 40 % with detector gain set to 110 to image CFP or YFP. Three fluorescence channels were collected for FRET imaging: Cerulean donor excitation and emission or DxDm, Cerulean donor excitation, Aphrodite acceptor emission or DxAm, and Aphrodite acceptor excitation and emission or AxAm. Accurate quantification requires sufficient signal-to-noise ratio, particularly in the DxDm channel which is less bright than DxAm. Variations in biosensor fluorescence and tissue-associated noise influence the signal-to-noise ratio; for example, autofluorescence and light scattering is higher in mature leaves compared to roots. Quantification of nuclear emission ratios was compared with control conditions and biosensor lines as noted to ensure sufficient signal-to-noise ratio.

A line average of four was used except for time course experiment shown in **Fig. 4H** where a higher line average was used. The z-stacks were acquired with a step-size of 1-3 µm depending upon the experiment.

Exogenous SA application in planta

Solution exchanges were performed on microscopy slide when the ¼ MS (pH 5.7) was replaced by desired solution, such as 10 µM SA in ¼ MS solution (83). Vacuum grease was used between the cover slip and the microscopy slide to create space for solution removal with fine tissue and solution addition with pipette. For rapid SA response in mature leaves, a fine needle (30Gx½, 0.3x13mm, TERUMO) was used to poke mature true leaves following with 2 µl ¼ MS (pH 5.7) as control vs 10 µM SA solution. The droplet was carefully dried by tissue after 5 mins and the sample is ready for imaging.

Salicylic acid quantification

Quantification of free SA was done based on assay with *Acinetobacter* sp. ADPWH_*lux* (50) with modifications. Bacteria were cultivated in liquid LB medium without antibiotics overnight at 37 °C on rotary shaker (120 rpm). At the day of measurement, fresh LB medium was mixed with bacterial culture (approx. 1:10) and cultivated at the same conditions until OD_{600}=0.4.

For quantification of free SA, plant material was collected into 2 ml Eppendorf tubes with 1 g of 1.3 mm ceramic beads and frozen in liquid nitrogen (50-150 mg FW). For the calibration curve preparation, 6 extra samples of untreated *NahG* plants were harvested. Frozen samples were homogenized in FastPrep-24 instrument (MP Biomedicals, USA) (40 s, 4.5 m/s) and frozen in liquid nitrogen. Then, NaAC (0.1 M, pH 5.6) buffer was added (250 µl per 100 mg FW) and the homogenisation step was repeated. Samples were centrifuged for 10 min at 15,000g at 4 °C, supernatant was collected into fresh tubes and kept on ice. Next, in sterile white microtiter plate with opaque bottom were mixed 60 µl LB, 50 µl of *Acinetobacter* sp. ADPWH_*lux* culture (OD_{600}=0.4) and 20 µl of plant extract or standard, with three technical replicates. Mixture was incubated 1 hour at 37 °C and luminescence was read on Tecan (Austria) microplate reader (well integration time 4 s). Standards were prepared by adding the known amount of SA (range 1-50 ng/mL) into untreated *NahG* plant extract. SA content was quantified based on a linear fitted calibration curve.

Nucleus localised FRET sensor image analysis

Image processing was performed using FRETENATOR2 toolset (*36*, *84*) for FIJI (*77*) with segmentation performed on the AxAm channel. Biosensor images were processed with *FRETENATOR segment and ratio v2.0* (https://github.com/JimageJ/FRETENATOR2). Segmentation settings were optimized but kept constant within each experiment. For segmentation, the Otsu thresholding algorithm was used, difference of Gaussian kernel size was determined empirically, and minimum ROI sizes were set between 15 to 100 to segmentate nuclei and avoiding noise. To determine whether DC3000 mCherry was proximal to a given nucleus, a custom plugin FRETENATOR segment and ratio v2.0 BT was written. After segmentation and processing of emission ratios, this program then dilates the label mask by 6 pixels, and mCherry is quantified in the dilated area.

Data visualisation and statistical analysis

Prism 10 (GraphPad Software) was used for plotting and statistical analysis. All statistical tests are described in the figure legends with sample size. Statistical data are provided in **Data S1**.

Fig. S1.

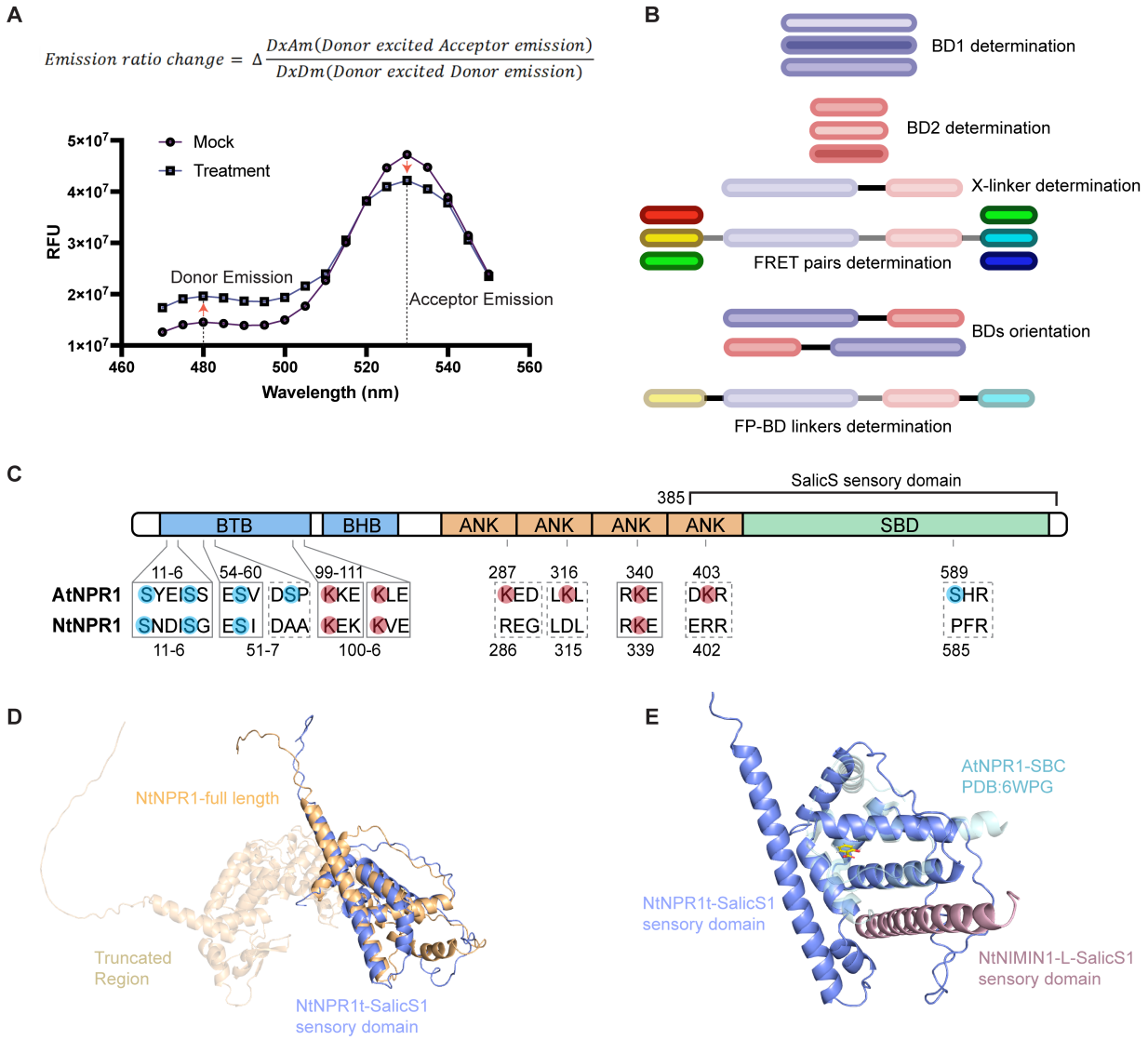

Fig. S1. Design FRET-based biosensor for SalicS1. (**A**) Equation to calculate change of emission ratio and emission spectrum for SalicS1. Emission spectrum of purified SalicS1 protein in response to 10 µM SA treatment showing an increase of donor emission peak at 480 nm and a decrease of acceptor emission peak at 530 nm. RFP: relative fluorescence units. (**B**) Cartoons of sensor screening process including determine Binding domains and their orientation, X linkers, FRET pairs and FP-BD linkers. (**C**) Summary of post-translational modification of AtNPR1 and NtNPR1. Sensory domain of SalicS is indicated in bracket. (**D**) AlphaFold3 predicted NtNPR1t-SalicS1 sensory domain overlap with NtNPR1- full length protein with truncated region indicated. (**E**) AlphaFold3 predicted SalicS1 sensory domain overlay with AtNPR1 SA binding core structure PDB:6WPG. SA molecule is indicated in yellow.

Fig. S2.

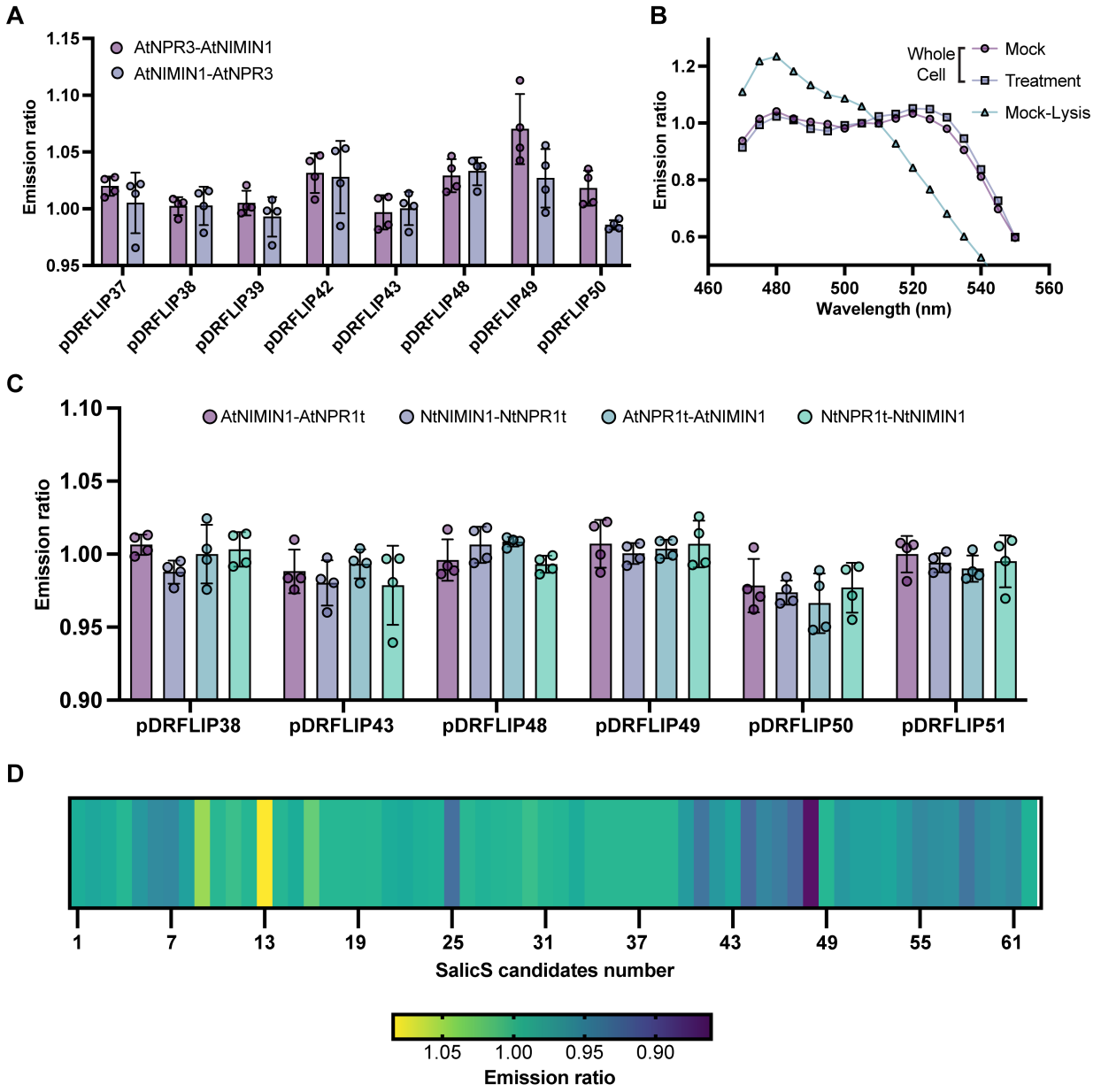

Fig. S2. Engineering and screening for SalicS1 candidates. (**A**) Full length AtNPR3 and AtNIMIN1 SA response test in whole yeast cells. Compositions of pDRFLIP vectors are listed in **Table S1**. (**B**) Emission spectrum curves of SalicS candidates in whole yeast cells vs cell lysates. (**C**) Combinatory screening with gateway screening platform. SalicS candidates with different sensory domain and FRET pairs were tested in cell lysates. Emission ratios were calculated upon 10 µM of SA application to the lysate. (**D**) Emission ratio of SalicS candidates upon 10 µM of SA application to optimize the sensor with Golden Gate-based screening platform. Candidate SalicS25 was chosen as final SalicS1 (**A&C**)**.** Error bars indicate SD. When a 5% emission ratio change is reached in the initial lysate screen, candidates were purified to be further characterised and engineered.

Fig. S3.

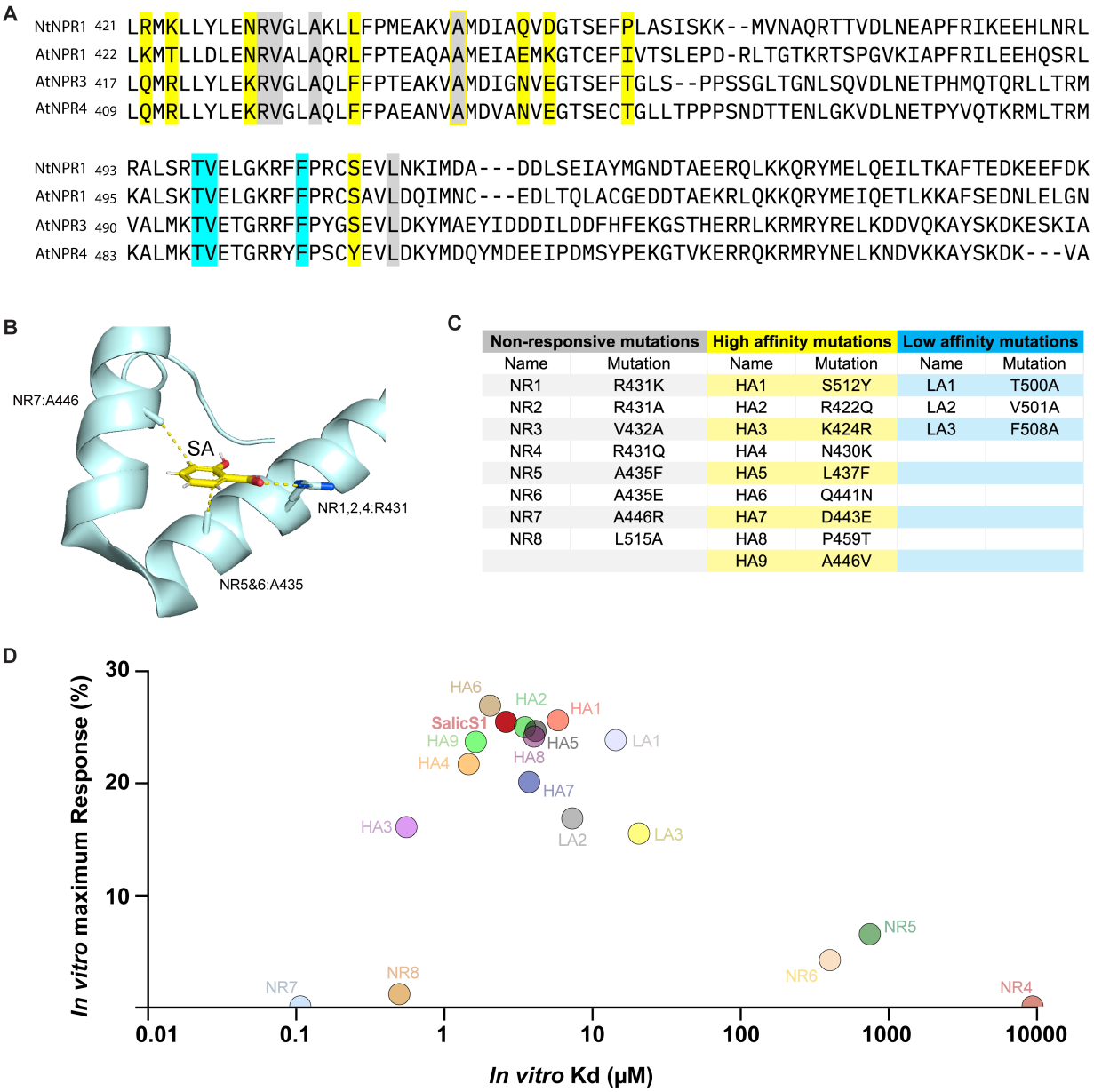

Non-responsive mutations		High affinity mutations		Low affinity mutations	
Name	Mutation	Name	Mutation	Name	Mutation
NR1	R431K	HA1	S512Y	LA1	T500A
NR2	R431A	HA2	R422Q	LA2	V501A
NR3	V432A	HA3	K424R	LA3	F508A
NR4	R431Q	HA4	N430K		
NR5	A435F	HA5	L437F		
NR6	A435E	HA6	Q441N		
NR7	A446R	HA7	D443E		
NR8	L515A	HA8	P459T		
		HA9	A446V		

Fig. S3. Design, Engineer and *in vitro* validation of SalicS variants. (**A**) Sequence alignment performed by Clustal Omega to align NtNRP1, AtNPR1, AtNPR3, and AtNPR4. Amino acids chosen for high affinity candidates are highlighted in yellow, non-responsive candidates are highlighted in grey, low affinity candidates are highlighted in blue. (**B**) Key amino acids R431, A435 and A446 are highlighted in the binding pocket interacting with SA. (**C**) Tables for final SalicS variants candidates. (**D**) Summary of maximum response and *Kd* for all SalicS variants.

Fig. S4.

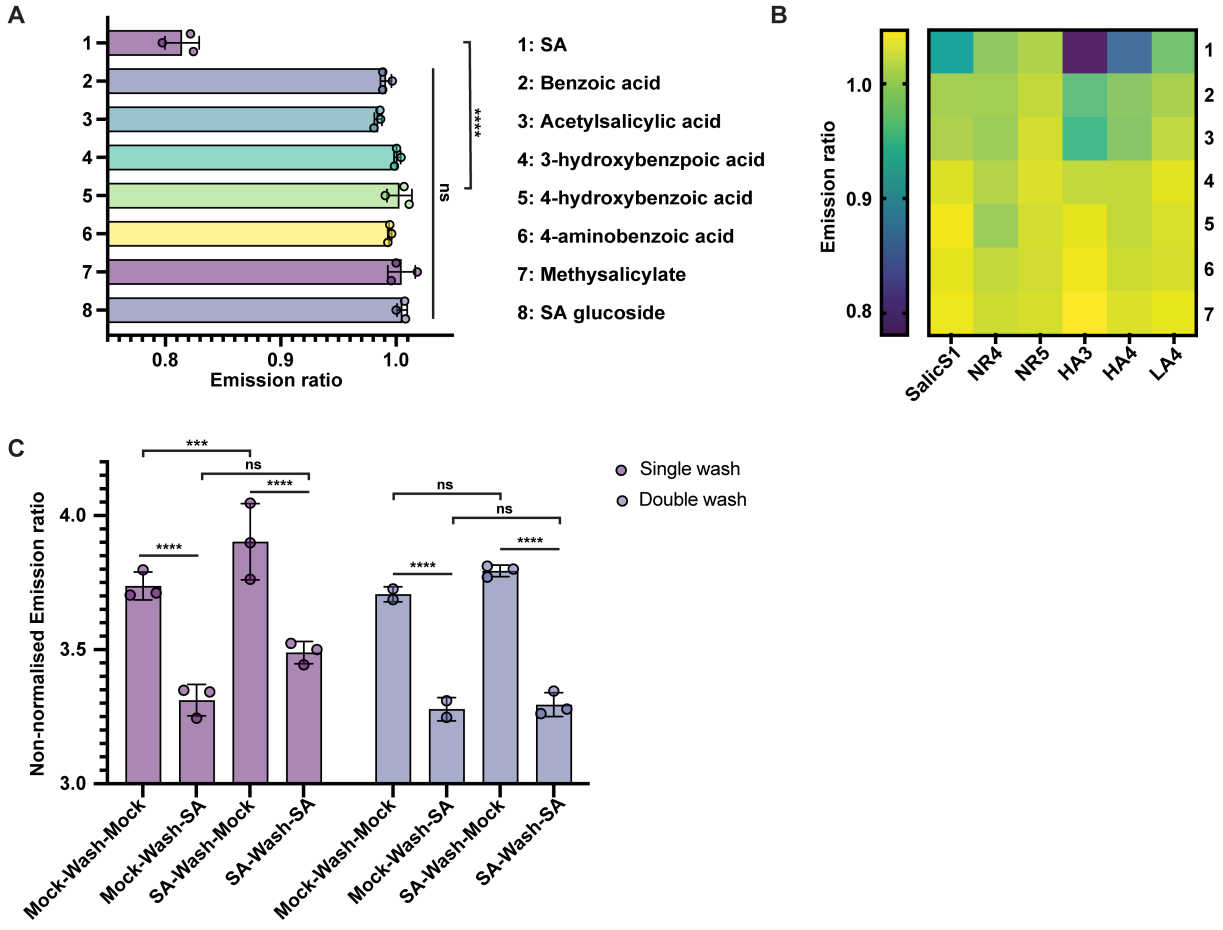

Fig. S4. SalicS1 *in vitro* specificity and reversibility test. (**A**) Specificity test of SalicS1 to SA and 7 different chemicals structurally like SA. *Turkey's multiple comparisons test, ****P value < 0.0001*, *ns = non-significant* (n=3). (**B**) Summary of specificity for the chosen NR4, NR5, HA3, HA4 and LA3 to different chemicals structurally like SA. (**C**) Reversibility test with double desalting column washes (20 mins interval from wash to data collection) vs single desalting column wash (5 mins interval from wash to data collection). *Šídák's multiple comparisons test, ****P value < 0.0001, ***P value < 0.001, ns = non-significant* (n=3). Exact P value, F value, degree of freedom for B and C are provided in **Data S1**.

Fig. S5.

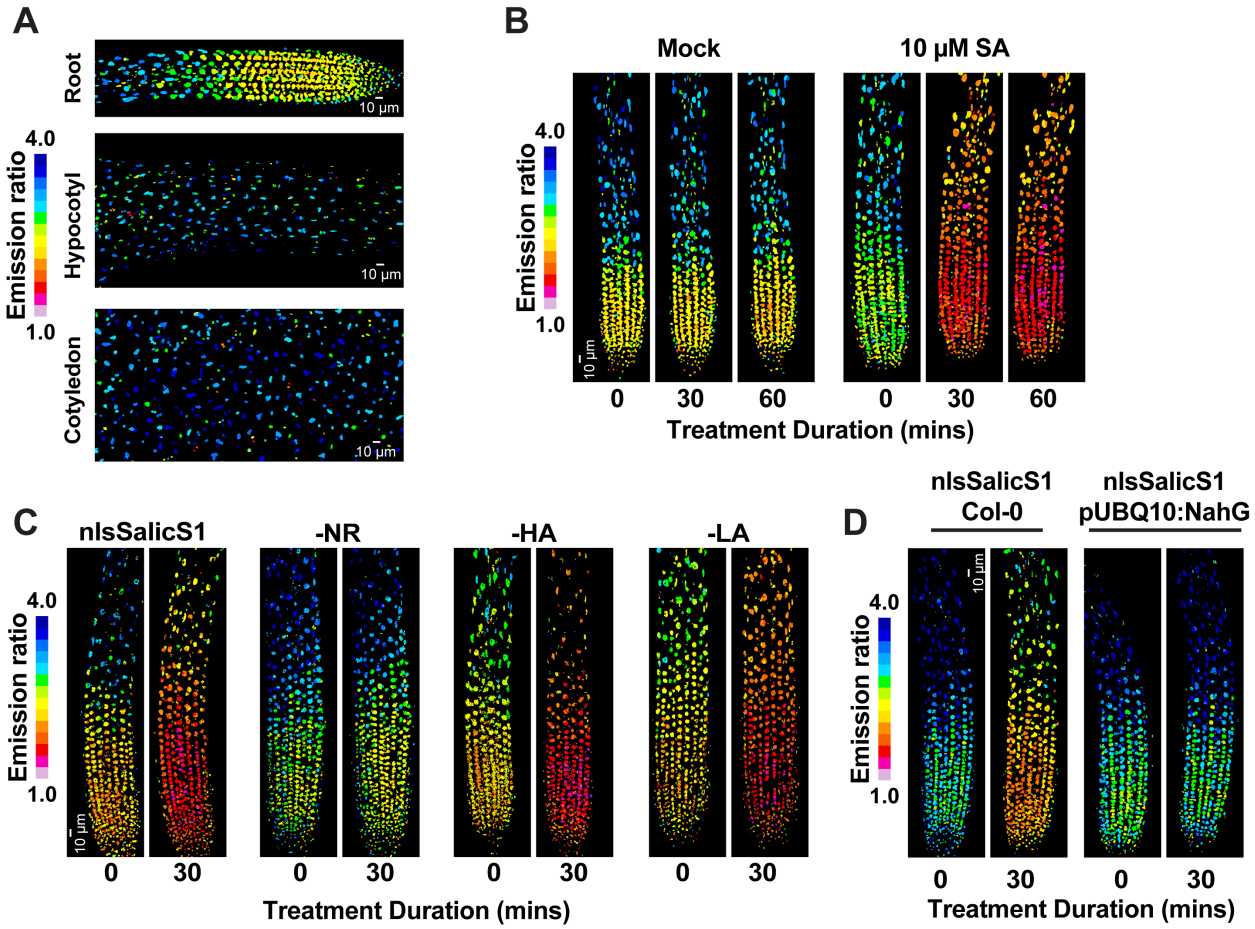

Fig. S5. Alternative LUTs images for Fig. 2: In planta validation for nlsSalicS1 in stably transformed Arabidopsis. (**A**) Endogenous pattern of SA reported by nlsSalicS1 in 5 days old seedlings at root, hypocotyl and cotyledon (LUT: 1.0-4.0, n=10). (**B**) nlsSalicS1 reported increased SA after exogenous 10 µM SA application. False coloured Images of roots before and after mock or 10 µM SA treatment (LUT: 1.0-4.0). (**C**) Representative images of nlsSalicS1, -HA, -LA and -NR reported different levels of emission ratio change when 10 µM exogenous SA was applied (LUT: 1.0-4.0). (**D**) Representative images of nlsSalicS1 when 10 µM SA was applied to pUBQ::NahG (overexpressed NahG) mutant (LUT:1.0-4.0).

Fig. S6.

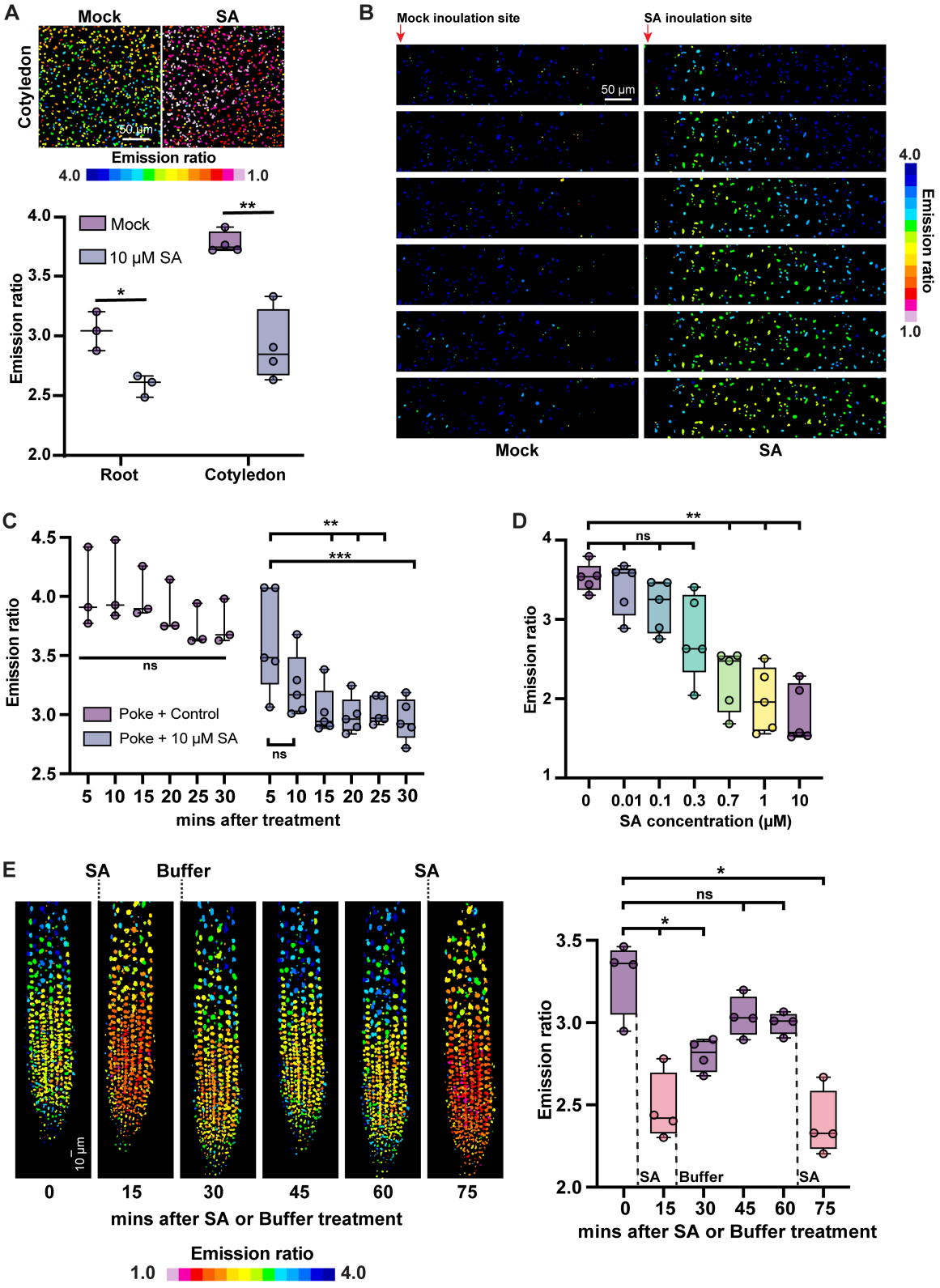
A
Mock
SA
Cotyledon
50 µm
Emission ratio
4.0
1.0
Mock
10 µM SA
Emission ratio
Root
Cotyledon
B
Mock inoulation site
SA inoulation site
50 µm
Mock
SA
Emission ratio
C
Emission ratio
Poke + Control
Poke + 10 µM SA
ns
mins after treatment
D
Emission ratio
SA concentration (µM)
E
SA
Buffer
SA
10 µm
mins after SA or Buffer treatment
Emission ratio
Emission ratio
SA
Buffer
SA
mins after SA or Buffer treatment

Fig. S6. nlsSalicS1 *in vivo* characterisation and reversibility test (**A**) Representative images of nlsSalicS1 reported SA accumulation in cotyledon during 10 µM SA treatment (LUT: 1.0-4.0). Quantification of emission ratio showed significant difference in emission ratio in both roots and cotyledons observed after 30 mins 10 µM SA treatment. *Repeated measure Two-way ANOVA, Uncorrected Fisher's LSD, *P value < 0.05, **P value < 0.005 (n=3, n=4).* (**B**) Representative images of nlsSalicS1 reported SA spread in 3 weeks old mature leaves (LUT: 1.0-4.0). (**C**) Quantification of nlsSalicS1 emission ratio of 3 weeks old mature leaves 5 - 30 minutes after needle poke plus addition of 1 µl of 10 µM SA vs mock solution. *Two-way ANOVA, Dunnett's multiple comparisons test, **P value < 0.005, ***P value = 0.0008*, *ns = non-significant P value > 0.05* (n=5,3). (**D**) Emission ratio of 5 days old nlsSalicS1 seedlings under different SA concentrations. *Repeated measure One-way ANOVA, Dunnett's multiple comparisons test, **P value < 0.005, ns = non-significant P value > 0.05 (n=5).* (**E**) In vivo reversibility test. Representative images and quantification of nlsSalicS1 reported SA accumulation in roots after 10 µM SA application and SA depletion after wash with buffer. Final SA application after 60 mins showed a similar nlsSalicS1 response compared to initial SA application. *Repeated measure One Way ANOVA, Dunnett's multiple comparisons test*, ** P value < 0.05, ns = non-significant* (n=4). Each point indicates the mean nuclear emission ratio for an individual root z-stack. For boxplots, centre line indicates median; box limits indicate upper and lower quartiles; whiskers indicate the upper/lower adjacent values. Exact P value, F value, degree of freedom are provided in **Data S1**.

Fig. S7.

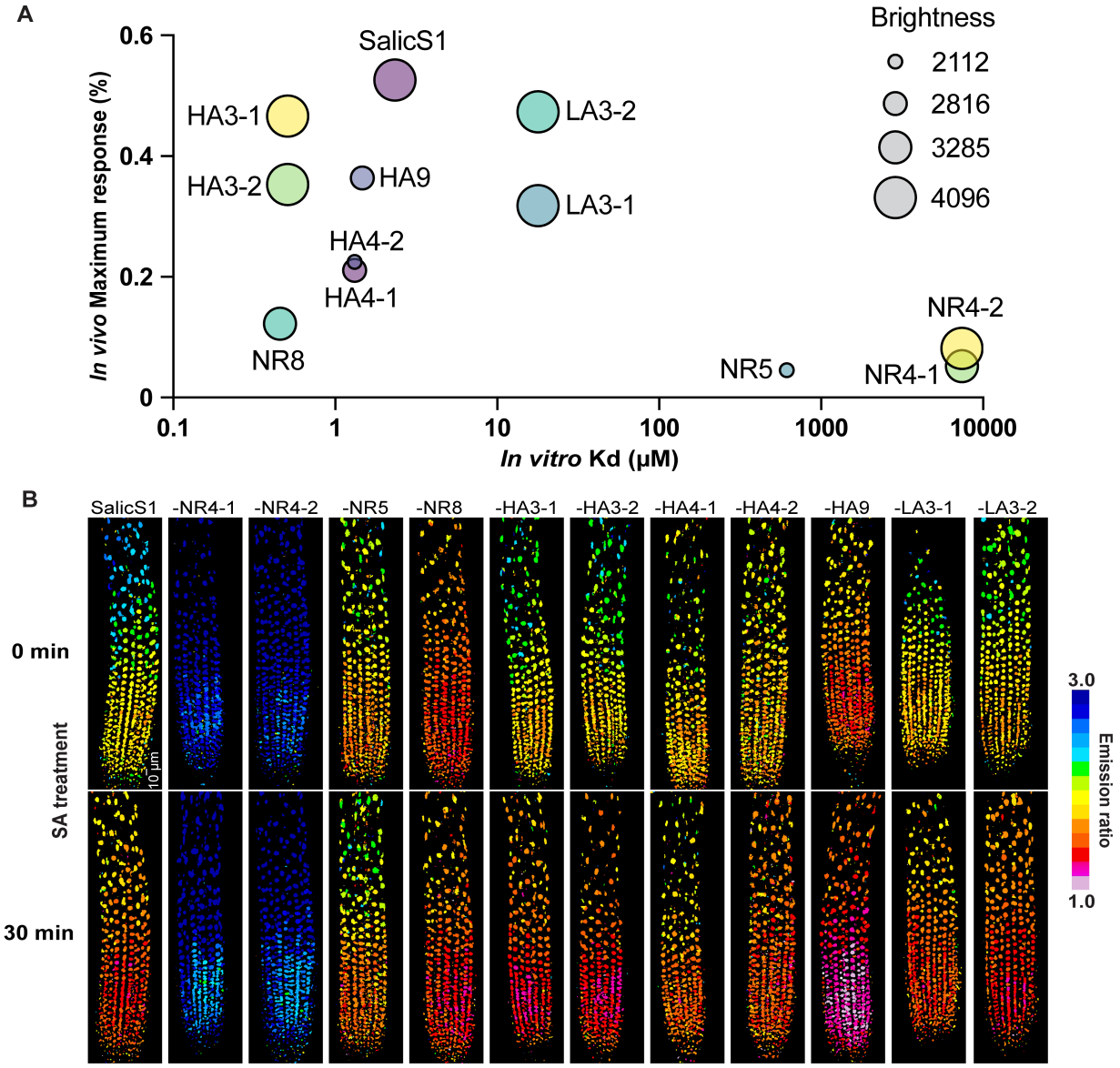

Fig. S7. nlsSalicS1 and variants in planta validation and screening. (**A**) Summary table for SalicS variants screen in planta. The size of the dot represents the highest brightness of DxDm (YFP channel) represents the expression level. The maximum response of variants in planta and affinity *in vitro* were summarized in the table (n=3). (**B**) nlsSalicS, -NR, -HA and -LA variants response to 10 μM exogenous SA treatment in 5 days Arabidopsis roots (n=3, LUT: 1.0-3.0).

Fig. S8.

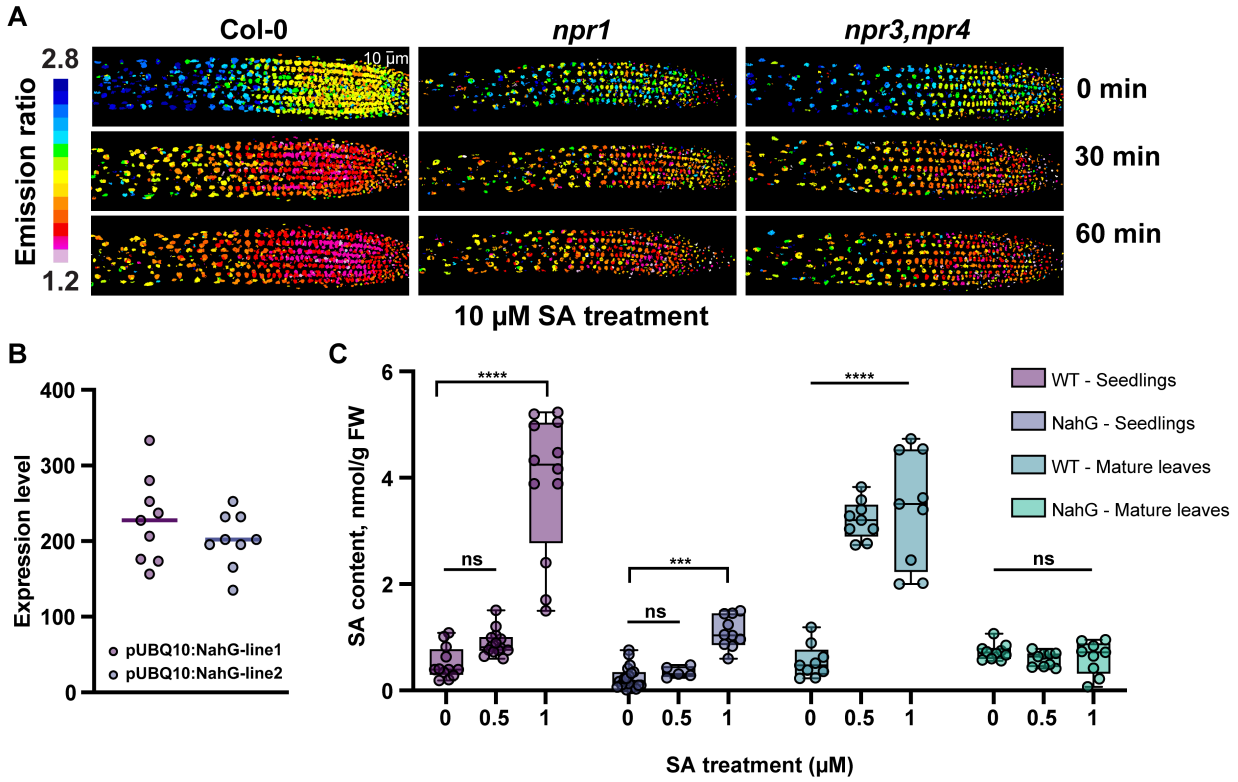

Fig. S8. nlsSalicS1 reported increased SA upon exogenous SA application in various signaling and biosynthesis mutants' background. (**A**) nlsSalicS1 reported increase of SA in Col-0 WT, *npr1* and *npr3,npr4* double mutants. Similar pattern and SA response were observed (n>3, LUT: 1.2-2.8). (**B**) qPCR quantification of expression of NahG in pUBQ10::NahG line-1 and line-2 (n=9). (**C**) SA quantification WT vs pUBQ:NahG seedlings and mature leaves by *Acinetobacter* sp. *ADPWH_lux* luminescence upon different SA concentration treatments. *Two-way ANOVA test, Dunnett's multiple comparisons test, **** P value < 0.0001, *** P value < 0.001, ns = non-significant* (n=12). Each point indicates the SA content for each biological replicates. For box plot, centre line indicates median; box limits indicate upper and lower quartiles; whiskers indicate the upper/lower adjacent values. Exact P value, F value, degree of freedom are provided in **Data S1**.

Fig. S9.

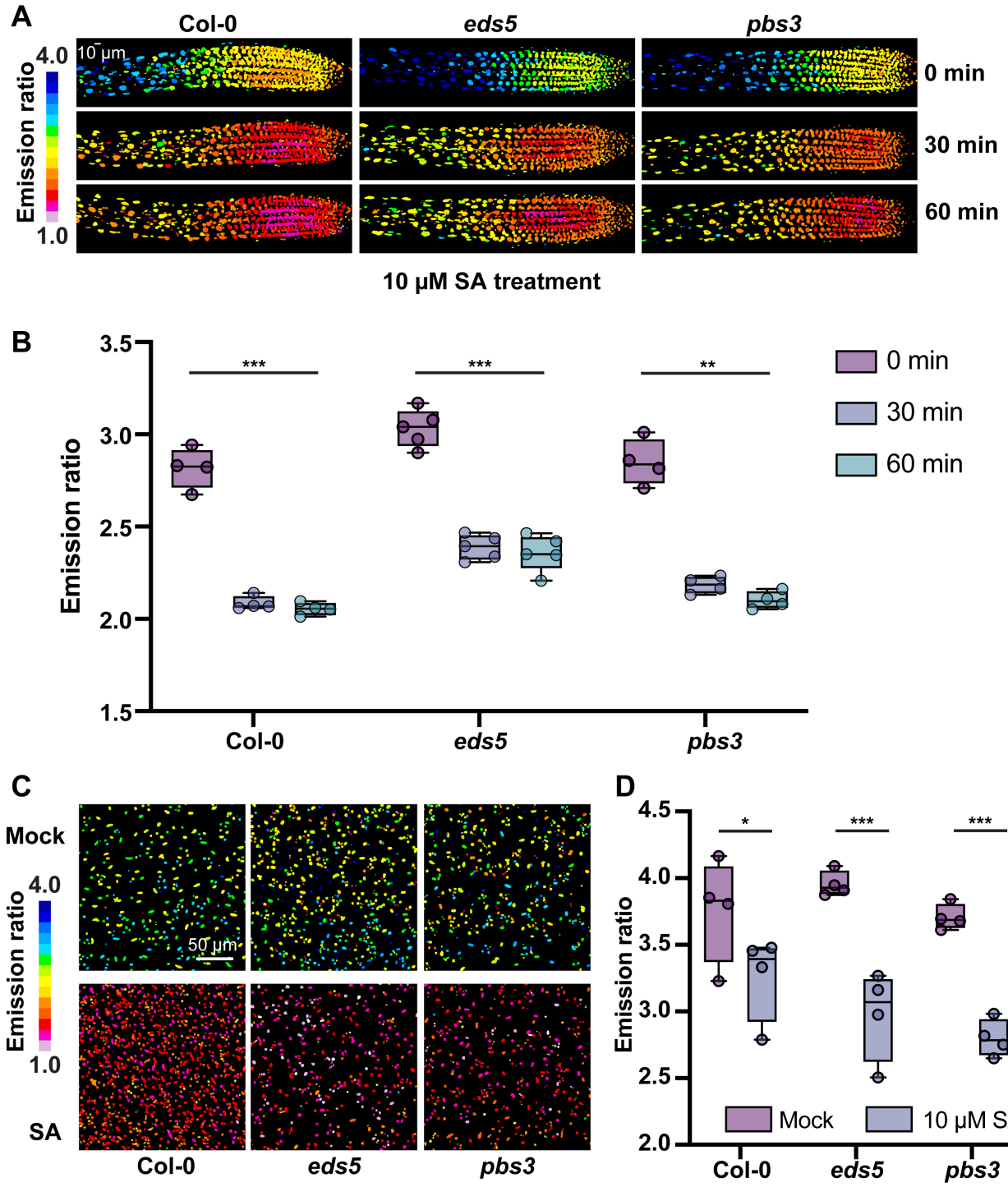

Fig. S9. nlsSalicS1 in biosynthesis mutants' background. (**A**) Representative images of nlsSalicS1 in WT Col-0, *eds5* and *pbs3* after 10 µM of SA treatment (LUT: 1.0-4.0). (**B**) Quantification of emission ratio change of nlsSalicS1 in Col-0 WT, *eds5* and *pbs3* after 10 µM of SA treatment for 30 mins and 60 mins in Arabidopsis roots in 5 days seedlings. *Repeated Measure Two-Way ANOVA, Dunnett's multiple comparisons test, ***P value < 0.001, **P value < 0.005* (n=4,5,4). Exact P value, F value, degree of freedom are provided in **Data S1**. (**C**) Representative images of

nlsSalicS in WT, *eds5* and *pbs3* after 3 hours 10 µM SA treatment in Arabidopsis mature leaves (LUT: 1.0-4.0). (**D**) Quantification of emission ratio change of nlsSalicS1 in Col-0 WT, *eds5* and *pbs3* after 10 µM of SA treatment for 3 hours in Arabidopsis mature leaves. *Two-Way ANOVA test, Šídák's multiple comparisons test, ***P value < 0.0005, *P value < 0.05* (n=4). Exact P value, F value, degree of freedom for B and C are provided in **Data S1**. **B & D:** Each point indicates the mean nuclear emission ratio for an individual root or cotyledon z-stack. For boxplots, centre line indicates median; box limits indicate upper and lower quartiles; whiskers indicate the upper/lower adjacent values.

Fig. S10.

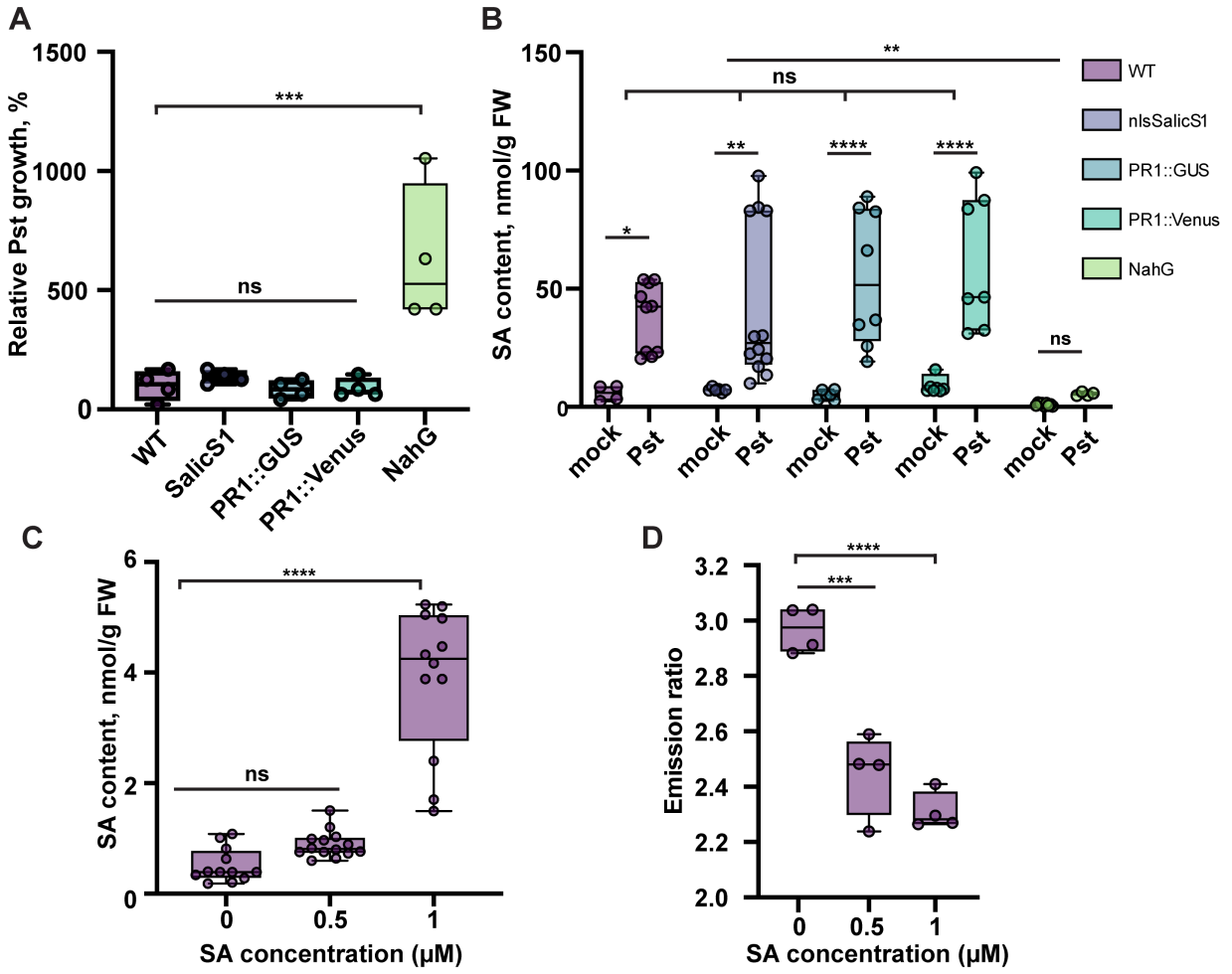

Fig. S10. Immunity test for nlsSalicS1 and other reporter lines and SA measurement in comparison with *Acinetobacter* sp. *ADPWH_lux* luminescence method. (**A**) Bacterial growth (CFU quantification) 2 days after *Pst* inoculation were quantified in WT, nlsSalicS1, PR1::GUS, PR1::Venus and NahG lines. *Ordinary One Way ANOVA test, Tukey's multiple comparisons test, ***P value < 0.0005* and *ns = non-significant* (n = 10,8,10,10,8). (**B**) Quantification of SA content with *Acinetobacter* sp. *ADPWH_lux* in nlsSalicS1 and reporter lines 2 days after *Pst* inoculation. *Two-Way ANOVA test, Šídák's multiple comparisons test, ****P value < 0.0001, **P value < 0.005, *P value < 0.05, ns = non-significant* (n = 10). No significant SA accumulation difference was detected between nlsSalicS1 and WT, PR1:GUS, PR1::Venus lines after Pst infection whereas significantly less SA accumulation was found in NahG overexpression line compared to nlsSalicS1. *Two-Way ANOVA test, Dunnett's multiple comparisons test, **P value < 0.01, ns = non-significant* (n = 6 for mock, n = 12 for *Pst* infection). (**C**) Quantification of SA content with *Acientobacter* sp. *ADPWH_lux* in nlsSalicS1 whole seedlings upon different concentrations of exogenous SA applications. *Two-Way ANOVA test, Dunnett's multiple comparison test, ***P value < 0.0001* (n > 12). (**D**) Quantification of emission ratio change of nlsSalicS1 root in seedlings upon different concentration of exogenous SA application. *Two-Way ANOVA test, Dunnett's multiple comparison test, ****P value < 0.0001, ***P value < 0.0005,* (n = 4). Each point indicates the mean nuclear emission ratio for an individual root z-stack. For boxplots, centre line indicates median; box limits indicate upper and lower quartiles; whiskers indicate the upper/lower adjacent values. **A-D**: Exact P value, F value, degree of freedom are provided in **Data S1**.

Fig. S11.

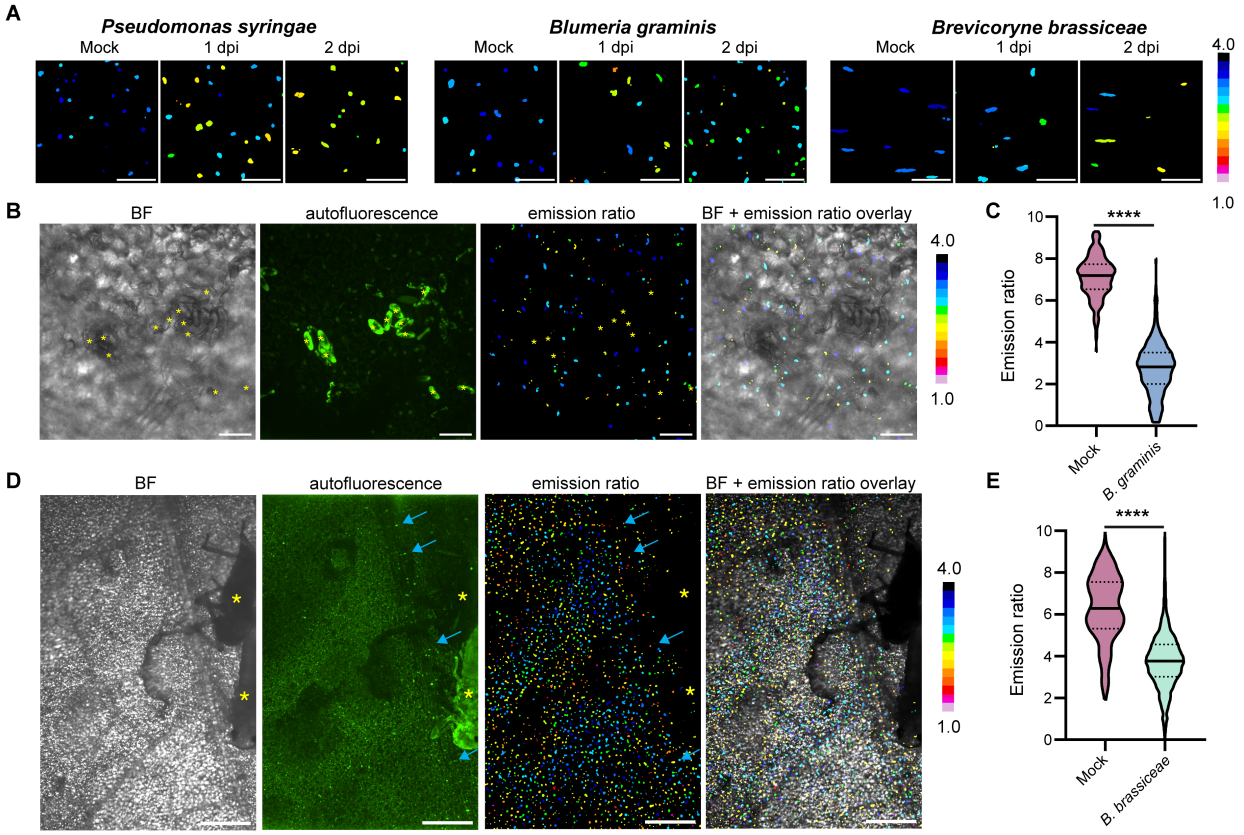

Fig. S11. nlsSalicS1 *in planta* validation upon different biotic stresses. (**A**) Representative images reported by nlsSalicS1 upon *P. syringae* pv *tomato* DC3000*, B. graminis* and *B. brassiceae* 1 and 2 dpi, scale bar = 50 µm. (LUT: 1.0-4.0). (**B&D**) Channel-by channel images depicting the placement of spores of *B. graminis* (scale bar 50 µm) and aphids *B. brassiceae* (scale bar 500 µm) on the leaf surface, and an overlay with the emission ratio. The asterisks indicate the spores/aphids, and arrows indicate the place of stylet penetration. (LUT: 1.0-4.0). (**C&E**) Emission ratio changes for all nucleus showed in images showed in B & D. *Unapired test with Welch's correction, ****P value<0.0001*.

Fig. S12.

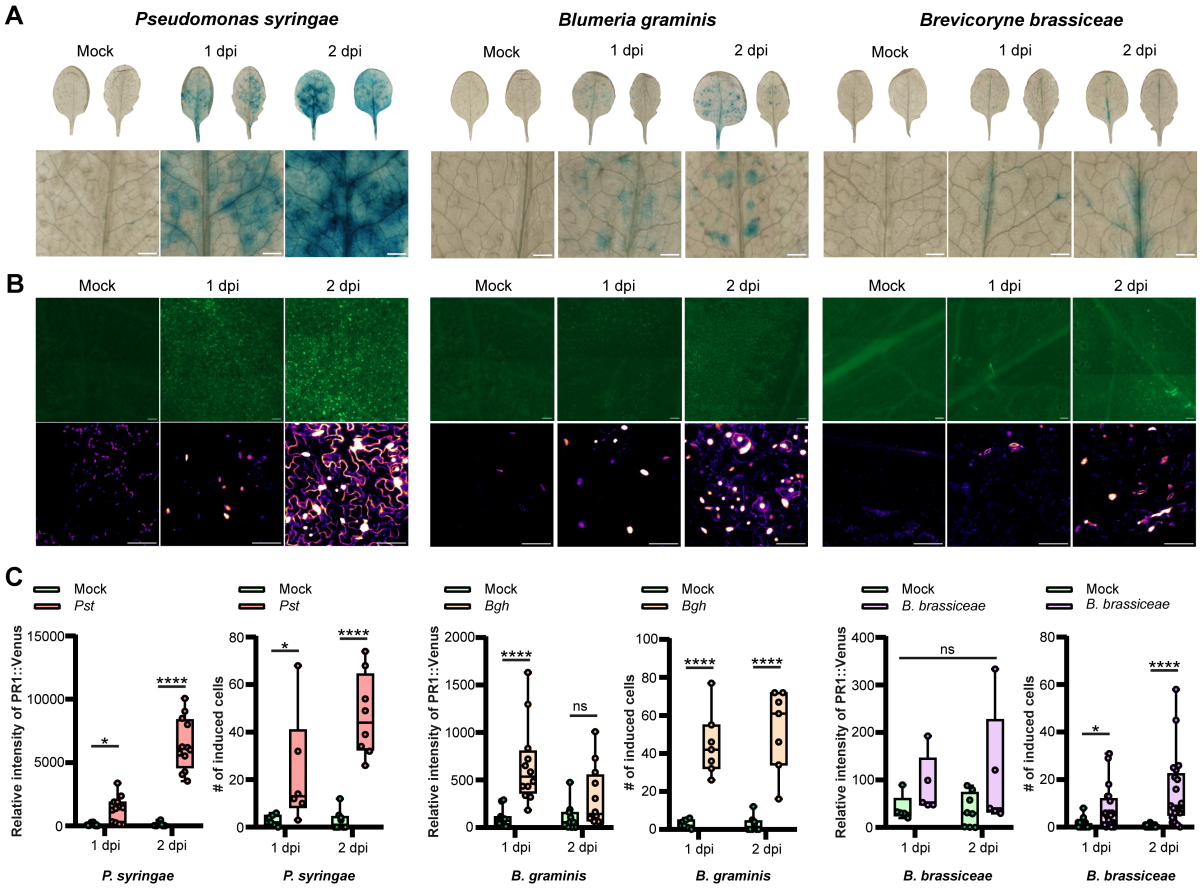

Fig. S12. nlsSalicS1 *in planta* validation upon different biotic stresses. (**A**) Representative images of pPR1 activation and SA quantification upon *P. syringae* pv *tomato* DC3000 (left), *B. graminis* (middle) and *B. brassiceae* (right) infection, 1- and 2-days post infection (dpi). pPR1::GUS visualisation in leaves and central leaf plate region (scale bar = 1 mm). (**B**) Representative images of pPR1::NLS3xVenus fluorescence obtained by widefield microscope (upper row, scale bar = 100 µm) and confocal microscope (lower row, scale bar = 50 µm). (**C**) Quantification of pPR1::NLS3xVenus associated fluorescence: relative intensity of fluorescence of 2,826 mm^2 leaf disc, and number of induced (PR1-positive) cells per 400 μm^2. At least 5 leaf discs and ROIs from three independent plants were assessed per treatment. *Two-way ANOVA with Sidak's multiple comparisons test; ns = non-significant, ****P value < 0.0001, *P value <0.05.*

Fig. S13.

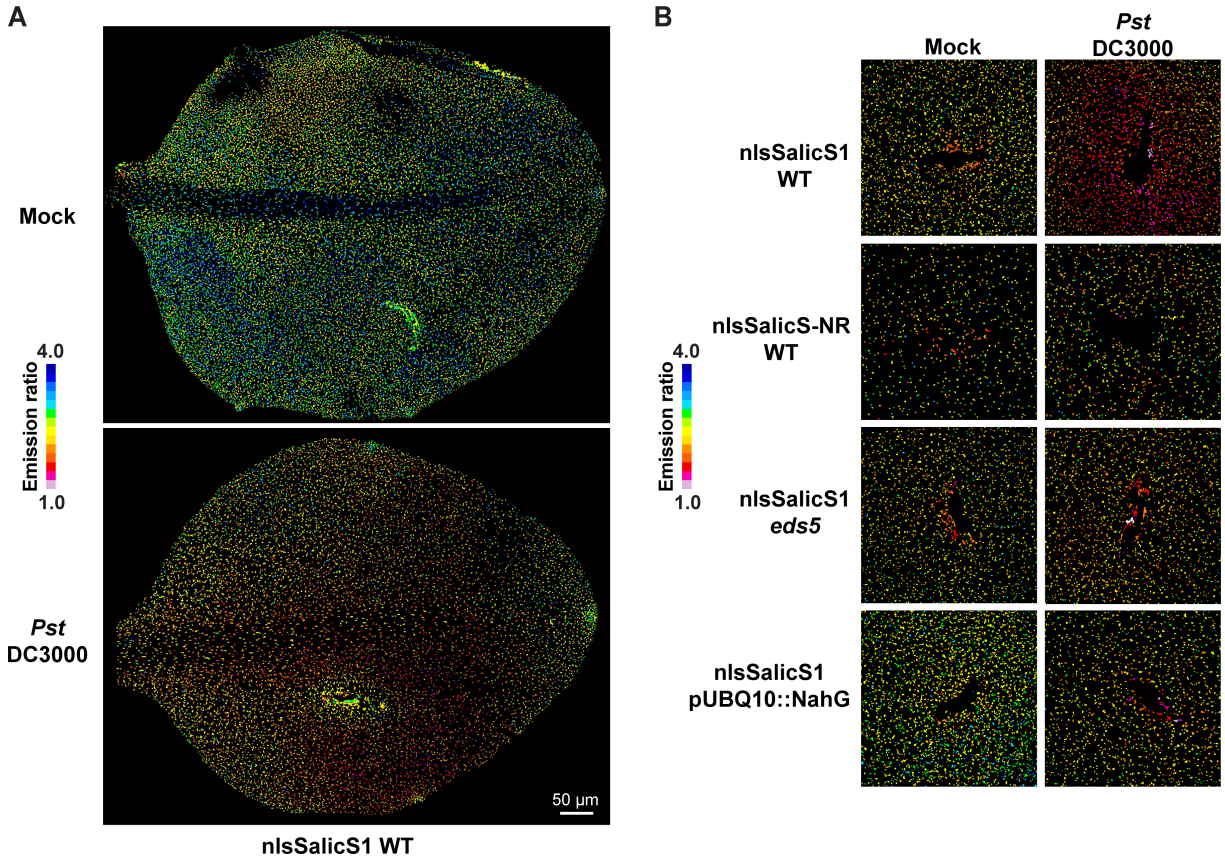

Fig. S13. Alternative LUTs images for Fig. 3: nlsSalicS1 reported SA accumulation under biotic stress (16 color LUT). (**A**) Represented images of 3 weeks old nlsSalicS1mature leaves under mock vs *Pst* DC3000 infection 20 hours after infection (n=3, LUT: 1.0-4.0). (B) Representative images for nlsSalicS1 WT Col-0 (n=6), nlsSalicS-NR WT Col-0 (n=6), nlsSalicS1 *eds5* (n=6) and nlsSalicS1-pUBQ10::NahG (n=8) upon mock (Left) vs *Pst* DC3000 (Right) inoculation 20 hrs post infection (hpi). (LUT: 1.0-4.0).

Fig. S14.

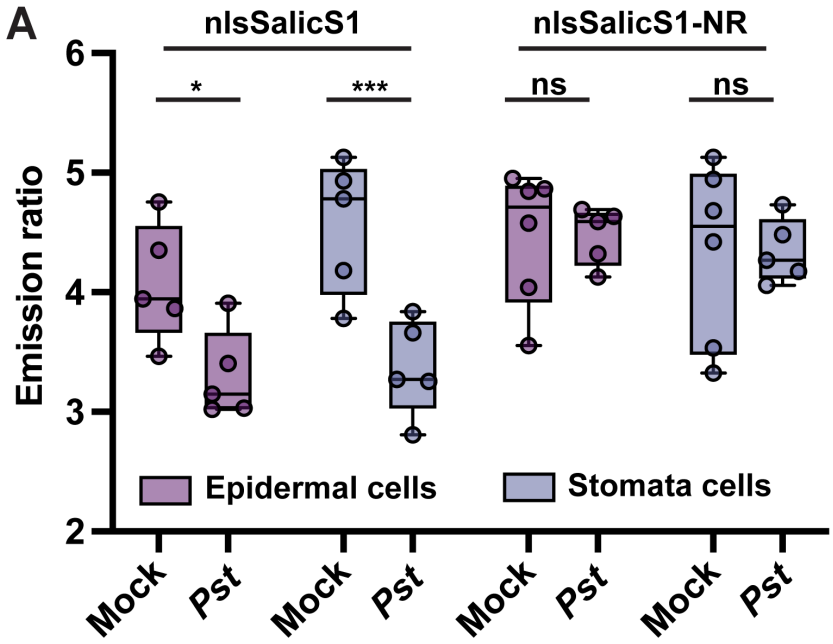

Fig. S14. Detailed spatiotemporal analysis of SA level under *Pst* infection. (**A**) Cellular resolution analysis showed no significant difference between stomata and epidermal cells in nlsSalicS1 and nlsSalicS1-NR. nlsSalicS1 reported SA accumulation in both epidermal cells and stomata cells 20 hpi of *Pst* DC3000-mCherry whereas nlsSalicS1-NR reported significant change. *Two-way ANOVA, Sidak's multiple comparisons test, ***P value = 0.0005, *P value = 0.0184, ns = non-significant* (n=5).

Fig. S15.

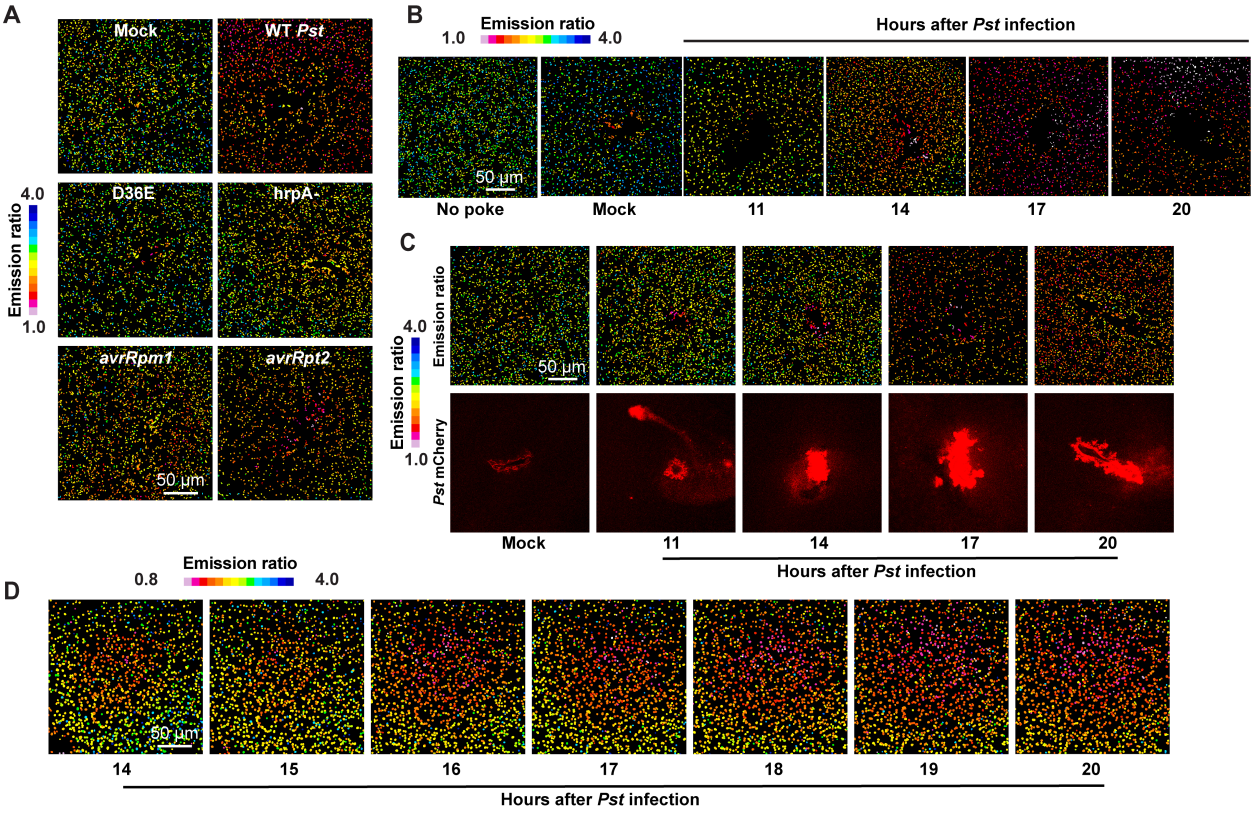

Fig. S15. Alternative LUTs images for Fig. 4: nlsSalicS1 reported SA in high spatiotemporal manner under *Pst* DC3000 infection (16 color LUT). (**A**) Representative images of nlsSalicS1 reported different emission ratio changes upon different *Pst* DC3000 mutant strains infection 20 hrs after infection. No poke (n=8), Mock poke (n=5), *Pst* DC3000 (n=9), D36E (n=8), *hrpA*- (n=9), *avrRpm1* (n=10), *avrRpt2* (n=10, LUT: 1.0-4.0). (**B**) Pseudo-time course of representative images for nlsSalicS1 in 3 weeks old mature leaves after infection (LUT: 1.0-4.0). (**C**) Representative images reported by nlsSalicS1 vs *Pst* DC3000-mCherry in pseudo-time course (LUT: 1.0-4.0). (**D**) nlsSalicS1 reported a surge of SA in Arabidopsis leaves spreading out from the infection site in a time course (n=3). After analysis, nuclei were dilated to allow easy visual discrimination at this magnification (LUT: 0.8-4.0).

Fig. S16.

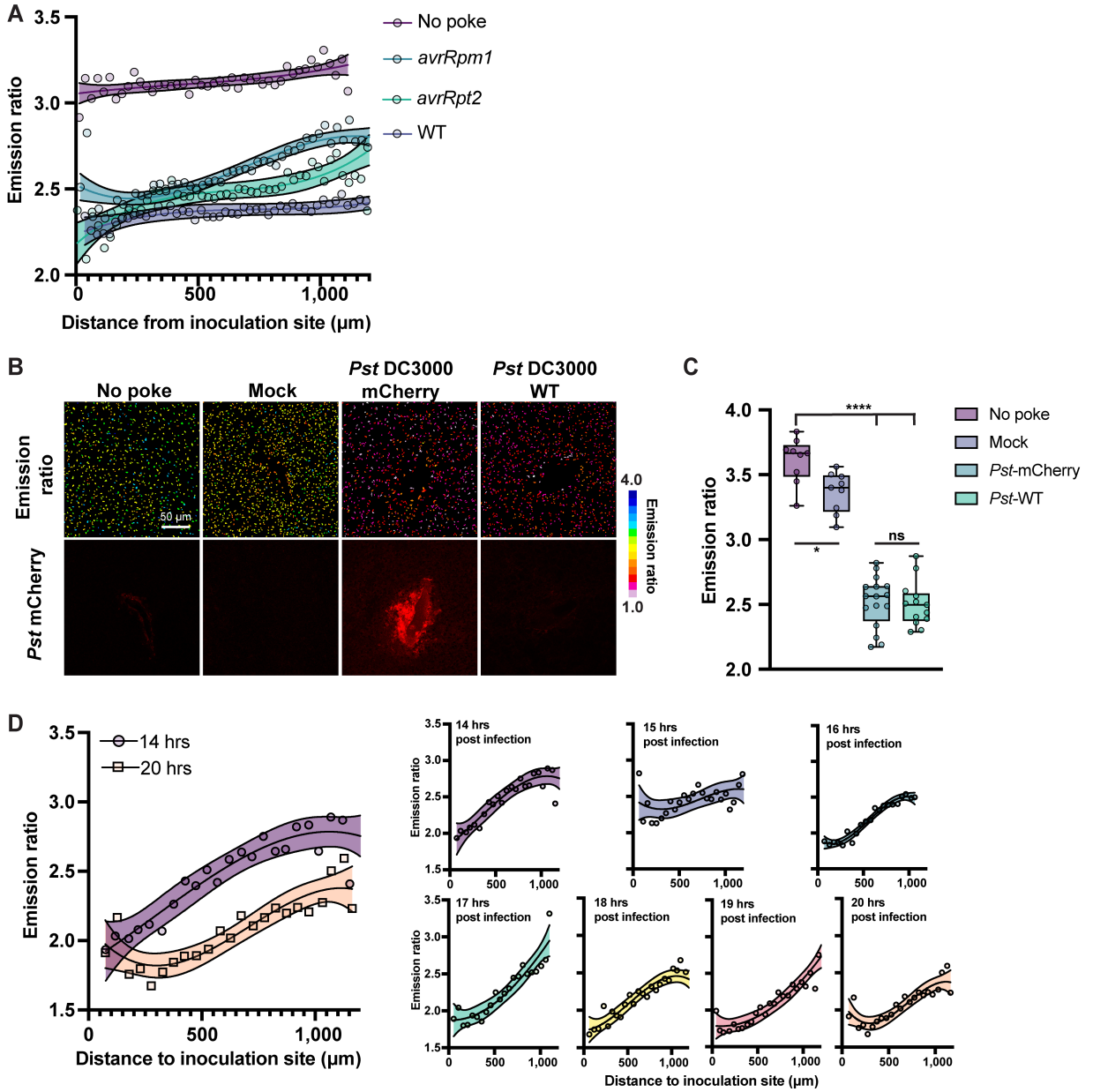

Fig. S16. Detailed spatiotemporal analysis of SA level under *Pst* infection. (**A**) Emission ratio of nlsSalicS1 under mock poke, *Pst* DC3000 WT, *avrRPM1* and *avrRpt2* variants treatment 20 hpi against the distance of nucleus to inoculation site. Non-linear third order polynomial fit, shaded area represented confidence band = 95% (n=8). (**B**) Representative images of nlsSalicS1 reported SA accumulation under Mock, *Pst* DC3000-mCherry and *Pst* DC3000 WT treatment (LUT: 1.0-4.0). RFP signal is only detected in *Pst* DC3000-mCherry. (**C**) Quantification of emission ratio showed no significant difference of emission ratio is observed between *Pst*-mCherry and *Pst*-WT *Pst* DC3000-mCherry and *Pst* DC3000-WT. *One-way ANOVA, Tukey's multiple comparisons test, ****P value < 0.001, * P value = 0.0271, ns = non-significant* (No poke: n=9, Mock: n=9, *Pst* DC3000-mCherry: n=16, *Pst* DC3000-WT: n=13). Exact P value, F value, degree of freedom are provided in **Data S1**. (**D**) Time course of emission ratio reported by nlsSalicS1 against the distance to inoculation site after *Pst* DC3000 inoculation. Non-linear third order polynomial fit, shaded area represented confidence band = 95% (n=3).

Fig. S17.

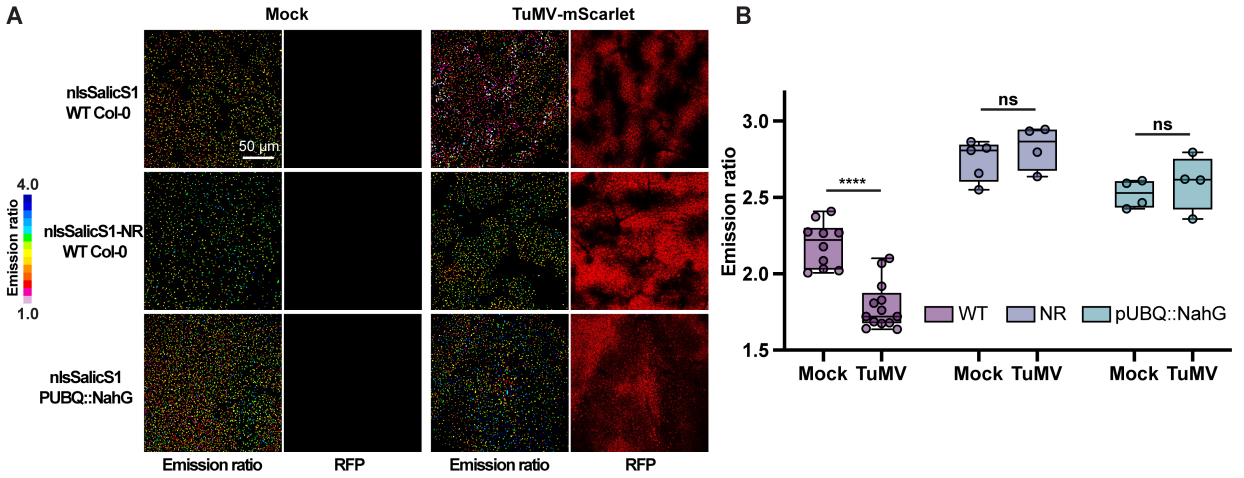

Fig. S17. nlsSalicS1 reported increased SA in distal leaves during TuMV infection (**A**) Representative images of nlsSalicS1, nlsSalicS1-NR and pUBQ::NahG lines in distal leaves 7-8 days after TuMV infection (LUT: 1.0-4.0). Infection was confirmed by detecting the viral 6K2:Scarlet protein (RFP channel). (**B**) Quantification of emission ratio change of nlsSalicS1, nlsSalicS1-NR and pUBQ10::NahG 7 days after TuMV infection. *Two Way ANOVA Test, Šídák's multiple comparisons test, ****P value < 0.0001, ns = non-significant* (n=10, n=13, n=5, n=4, n=4, n=4). Each point indicates the mean nuclear emission ratio for an individual root or cotyledon z-stack. For boxplots, centre line indicates median; box limits indicate upper and lower quartiles; whiskers indicate the upper/lower adjacent values. Exact P value, F value, degree of freedom is provided in **Data S1**.

Table S1.

Destination Vector			Sensory Domain					
Name	1st FP	2nd FP	AtNPR3-AtNIMIN1	AtNIMIN1-AtNPR3	AtNIMIN1-L-AtNPR1t	NtNIMIN1-L-NtNPR1t	AtNPR1t-AtNIMIN1-L	NtNPR1t-NtNIMIN1-L
pDRFLIP37	Cit	Cer	1.002	1.003	N/A	N/A	N/A	N/A
pDRFLIP38	edCit	edCer	1.005	0.993	1.006	0.988	1.000	1.003
pDRFLIP39	edAFPt9	t7edCFPt9	1.031	1.028	N/A	N/A	N/A	N/A
pDRFLIP42	Cit	mCer	0.997	1.000	N/A	N/A	N/A	N/A
pDRFLIP43	edAFPt9	edCer	1.029	1.033	0.986	0.989	0.998	0.968
pDRFLIP48	AFPt9	mTrq2	1.070	1.027	0.998	1.003	1.008	0.996
pDRFLIP49	AFPt9	t7mTrq2t9	1.018	0.986	0.999	1.005	1.004	1.010
pDRFLIP50	edAFPt9	t7edTrq2t9	1.002	1.003	0.972	0.977	0.982	0.965
pDRFLIP51	edAFPt9	edTrq2	N/A	N/A	0.999	1.000	0.996	0.984

Design #	N-tag	First fluorescent protein	Second fluorescent protein	C-tag	pDRFLIP for yeast expression
37	6H	Cit	Cer	cMyc	Yes
38	6H	edCit	edCer	cMyc	Yes
39	6H	edAFPt9	t7edCFPt9	cMyc	Yes
42	6H	Cit	mCer	cMyc	Yes
43	6H	edAFPt9	edCer	cMyc	Yes
48	6H	AFPt9	mTrq2	cMyc	Yes
49	6H	AFPt9	t7mTrq2t9	cMyc	Yes
50	6H	edAFPt9	t7edTrq2t9	cMyc	Yes
51	6H	edAFPt9	edTrq2	cMyc	Yes

Abbreviation	Full name	Notes
AFP	Aphrodite	Yellow (codon changed Venus)
Cit	Citrine	Yellow
Cer	Cerulean	Blue
Trq	Turquoise	Blue
ed	enhanced dimer	dimer tendency variant
m	monomeric	dimer tendency variant
t#	truncation	N- or C- terminal
w/out ed or m	weak dimer	original eGFP

Table S1. Description of SalicS1 candidate constructs. Gateway cloning platform are first used to determine SalicS1 sensory domain candidates. *In vitro* emission ratio of SA response of pDRFLIP# with different sensory domain were listed in the top table. Description of the tags and fluorescence protein pairs of different pDRFLIP# were described in the middle table. Abbreviation of different Fluorescence proteins used were described in the bottom table.

Table S2.

Level	Position	Constructs	FP-BD linker	N-terminal	C-terminal	FP-BD linker
Level -1	M1	edAFPt9	SS	AATG	TTCG	SS
Level -1	M1	edAFPt9	PP	AATG	TcCG	SP
Level -1	M1	edAFPt9	SP	AATG	TcCG	SP
Level -1	M1	AausFP1	PP	AATG	TcCG	PP
Level -1	M1	AausFP1	SP	AATG	TcCG	SP
Level -1	M1	Gamillus	PP	AATG	TcCG	PP
Level -1	M1	Gamillus	SP	AATG	TcCG	SP
Level -1	M1	mKOk	PP	AATG	TcCG	PP
Level -1	M1	mKOk	SP	AATG	TcCG	SP
Level -1	M1	mScarlet	PP	AATG	TcCG	PP
Level -1	M1	mScarlet	SP	AATG	TcCG	SP
Level -1	M1	TagRFP	PP	AATG	TcCG	PP
Level -1	M1	TagRFP	SP	AATG	TcCG	SP
Level -1	M1	mCer3	PP	AATG	TcCG	PP
Level -1	M1	mCer3	SP	AATG	TcCG	SP
Level -1	M1	mTagBFP2	PP	AATG	TcCG	PP
Level -1	M1	mTagBFP2	SP	AATG	TcCG	SP
Level -1	M2	NtNPR1	PP	TcCG	AGGT	SS
Level -1	M2	NtNIMIN1L	PP	TcCG	AGGT	SS
Level -1	M3	L12	GG	AGGT	GGAG	GG
Level -1	M3	L52	GG	AGGT	GGAG	GG
Level -1	M3	L64	GG	AGGT	GGAG	GG
Level -1	M3	L72	GG	AGGT	GGAG	GG
Level -1	M3	L89	GG	AGGT	GGAG	GG
Level -1	M3	L95	GG	AGGT	GGAG	GG
Level -1	M3	L118	GG	AGGT	GGAG	GG
Level -1	M3	L258	GG	AGGT	GGAG	GG
Level -1	M4	NtNPR1	GG	GGAG	cCTc	SS
Level -1	M4	NtNIMIN1L	GG	GGAG	cCTc	SS
Level -1	M5	edCer	SS	TCTT	GCTT	SS
Level -1	M5	edCer	PP	CCTC	GCTT	PP
Level -1	M5	edCer	PL	CCTC	GCTT	PL
Level -1	M5	AausFP1	PP	CCTC	GCTT	PP
Level -1	M5	AausFP1	PL	CCTC	GCTT	PL
Level -1	M5	Gamillus	PP	CCTC	GCTT	PP
Level -1	M5	Gamillus	PL	CCTC	GCTT	PL
Level -1	M5	mKOk	PP	CCTC	GCTT	PP

Level -1	M5	mKOk	PL	CCTC	GCTT	PL
Level -1	M5	mScarlet	PP	CCTC	GCTT	PP
Level -1	M5	mScarlet	PL	CCTC	GCTT	PL
Level -1	M5	TagRFP	PL	CCTC	GCTT	PP
Level -1	M5	TagRFP	PL	CCTC	GCTT	PL
Level -1	M5	mCer3	PP	CCTC	GCTT	PP
Level -1	M5	mCer3	PL	CCTC	GCTT	PL
Level -1	M5	mTagBFP2	PP	CCTC	GCTT	PP
Level -1	M5	mTagBFP2	PL	CCTC	GCTT	PL
Level -1	M5	edCer3	PL	CCTC	GCTT	PL
Level -1	M5	edCer3-NdeI1	PL	CCTC	GCTT	PL
Level -1	M5	edCer3-NdeI2	PL	CCTC	GCTT	PL
Level -1	M5	edCer3-NdeI3	PL	CCTC	GCTT	PL
Level -1	M5	edCer3-NdeI4	PL	CCTC	GCTT	PL
Level -1	M5	edCer3-NdeI5	PL	CCTC	GCTT	PL
Level -1	M5	edCer3-NdeI6	PL	CCTC	GCTT	PL
Level -1	M5	edCer3-NdeI7	PL	CCTC	GCTT	PL
Level -1	M5	edCer3-NdeI8	PL	CCTC	GCTT	PL
Level -1	M5	edCer3-NdeI9	PL	CCTC	GCTT	PL
Level -1	M5	WTCer3	PL	CCTC	GCTT	PL
Level -1	M5	WTCer3-NdeI1	PL	CCTC	GCTT	PL
Level -1	M5	WTCer3-NdeI2	PL	CCTC	GCTT	PL
Level -1	M5	WTCer3-NdeI3	PL	CCTC	GCTT	PL
Level -1	M5	WTCer3-NdeI4	PL	CCTC	GCTT	PL
Level -1	M5	WTCer3-NdeI5	PL	CCTC	GCTT	PL
Level -1	M5	WTCer3-NdeI6	PL	CCTC	GCTT	PL
Level -1	M5	WTCer3-NdeI7	PL	CCTC	GCTT	PL
Level -1	M5	WTCer3-NdeI8	PL	CCTC	GCTT	PL
Level -1	M5	WTCer3-NdeI9	PL	CCTC	GCTT	PL
Level -1	M5	edTRQ2	PL	CCTC	GCTT	PL
Level -1	M5	edTRQ2-NdeI1	PL	CCTC	GCTT	PL
Level -1	M5	edTRQ2-NdeI2	PL	CCTC	GCTT	PL
Level -1	M5	edTRQ2-NdeI3	PL	CCTC	GCTT	PL
Level -1	M5	edTRQ2-NdeI4	PL	CCTC	GCTT	PL
Level -1	M5	edTRQ2-NdeI5	PL	CCTC	GCTT	PL
Level -1	M5	edTRQ2-NdeI6	PL	CCTC	GCTT	PL
Level -1	M5	edTRQ2-NdeI7	PL	CCTC	GCTT	PL

Table S2. Golden-Gate Level -1 modules. The library of Level -1 modules for FRET-based sensor screening platform. Overhangs and linkers for each module are described.

Table S3.

Linker	Structure	Description
L12		Short flexible linker rich in A, G, S
L52		Mid-length spring linker 8xGPGGA repeats
L65	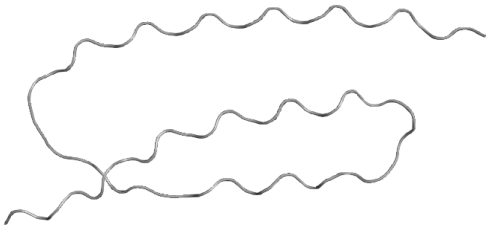	Mid-length flexible linker 9xGGSGGS repeats
L71		Short rigid Alpha-helix 11xMALEK repeats

L89	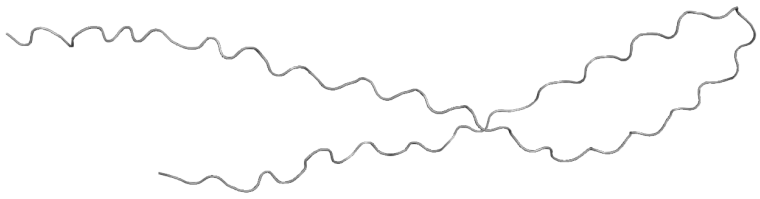	Long flexible linker
L95		Mid-length alpha-helix linker
L118		Long alpha-helix linker Spring linker
L256	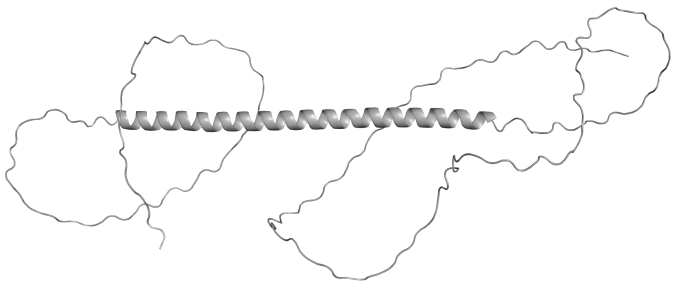	Super long alpha-helix linker

Table S3. Structures and descriptions of all X-linkers used in SalicS screening. Structures of X-linkers are predicted with AlphaFold3 and their best model are presented with their description of length of flexibilities.

Table S4.

Name	FP1	FP-BD linker	BD1	X-linker	BD2	FP-BD linker	FP2	Emission ratio
ggSalicS_001	edAFPt9	PP	NtNIMIN1-L	L12	NtNPR1	PP	edCer	0.99
ggSalicS_002	edAFPt9	PP	NtNIMIN1-L	L52	NtNPR1	PP	edCer	0.98
ggSalicS_003	edAFPt9	PP	NtNIMIN1-L	L64	NtNPR1	PP	edCer	0.99
ggSalicS_004	edAFPt9	PP	NtNIMIN1-L	L71	NtNPR1	PP	edCer	1.00
ggSalicS_005	edAFPt9	PP	NtNPR1	L12	NtNIMIN1-L	PP	edCer	0.96
ggSalicS_006	edAFPt9	PP	NtNPR1	L52	NtNIMIN1-L	PP	edCer	0.95
ggSalicS_007	edAFPt9	PP	NtNPR1	L64	NtNIMIN1-L	PP	edCer	0.95
ggSalicS_008	edAFPt9	PP	NtNPR1	L71	NtNIMIN1-L	PP	edCer	0.98
ggSalicS_009	Gamillust6	PP	NtNIMIN1-L	L12	NtNPR1	PP	TagRFP	1.05
ggSalicS_010	TagRFP	PP	NtNIMIN1-L	L12	NtNPR1	PP	Gamillust6	1.00
ggSalicS_011	TagRFP	PP	NtNIMIN1-L	L12	NtNPR1	PP	AausFP1	1.01
ggSalicS_012	AausFP1	PP	NtNIMIN1-L	L12	NtNPR1	PP	TagRFP	1.00
ggSalicS_013	Gamillust6	PP	NtNPR1	L12	NtNIMIN1-L	PP	TagRFP	1.08
ggSalicS_014	TagRFP	PP	NtNPR1	L12	NtNIMIN1-L	PP	Gamillust6	1.00
ggSalicS_015	TagRFP	PP	NtNPR1	L12	NtNIMIN1-L	PP	AausFP1	0.99
ggSalicS_016	AausFP1	PP	NtNPR1	L12	NtNIMIN1-L	PP	TagRFP	1.03
ggSalicS_017	edAFPt9	PP	NtNIMIN1-L	L118	NtNPR1	PP	edCer	1.00
ggSalicS_018	edAFPt9	PP	NtNIMIN1-L	L89	NtNPR1	PP	edCer	1.00
ggSalicS_019	edAFPt9	PP	NtNIMIN1-L	L95	NtNPR1	PP	edCer	1.00
ggSalicS_020	edAFPt9	PP	NtNIMIN1-L	L248	NtNPR1	PP	edCer	1.00
ggSalicS_021	edAFPt9	PP	NtNPR1	L118	NtNIMIN1-L	PP	edCer	0.99
ggSalicS_022	edAFPt9	PP	NtNPR1	L89	NtNIMIN1-L	PP	edCer	0.98
ggSalicS_023	edAFPt9	PP	NtNPR1	L95	NtNIMIN1-L	PP	edCer	0.99
ggSalicS_024	edAFPt9	PP	NtNPR1	L248	NtNIMIN1-L	PP	edCer	0.99
ggSalicS_025	edAFPt9	SP	NtNPR1	L52	NtNIMIN1-L	PL	edCer	0.92
ggSalicS_026	AausFP1	SP	NtNPR1	L52	NtNIMIN1-L	PL	TagRFP	1.00
ggSalicS_027	TagRFP	SP	NtNPR1	L52	NtNIMIN1-L	PL	Gamillust6	0.99
ggSalicS_028	Gamillust6	SP	NtNPR1	L52	NtNIMIN1-L	PL	TagRFP	1.00
ggSalicS_029	TagRFP	SP	NtNPR1	L52	NtNIMIN1-L	PL	AausFP1	1.00
ggSalicS_030	mTagBFP2	SP	NtNPR1	L52	NtNIMIN1-L	PL	Gamillus	1.01
ggSalicS_031	mTagBFP2	SP	NtNPR1	L52	NtNIMIN1-L	PL	AausFP1	1.00
ggSalicS_032	Gamillus	SP	NtNPR1	L52	NtNIMIN1-L	PL	mTagBFP2	1.00

ggSalicS_033	AausFP1	SP	NtNPR1	L52	NtNIMIN1-L	PL	mTagBFP2	0.99
ggSalicS_034	mCerulean3	SP	NtNPR1	L52	NtNIMIN1-L	PL	mKOK	1.00
ggSalicS_035	mCerulean3	SP	NtNPR1	L52	NtNIMIN1-L	PL	mScarlet	1.00
ggSalicS_036	mCerulean3	SP	NtNPR1	L52	NtNIMIN1-L	PL	TagRFP	1.00
ggSalicS_037	mKOK	SP	NtNPR1	L52	NtNIMIN1-L	PL	mCerulean3	1.00
ggSalicS_038	mScarlet	SP	NtNPR1	L52	NtNIMIN1-L	PL	mCerulean3	1.00
ggSalicS_039	TagRFP	SP	NtNPR1	L52	NtNIMIN1-L	PL	mCerulean3	1.00
ggSalicS_040	edAFPt9	SP	NtNPR1	L52	NtNIMIN1-L	PL	mCer3	0.97
ggSalicS_041	edAFPt9	SP	NtNPR1	L52	NtNIMIN1-L	PL	edCer3	0.93
ggSalicS_042	edAFPt9	SP	NtNPR1	L52	NtNIMIN1-L	PL	edCer3Ndel1	0.96
ggSalicS_043	edAFPt9	SP	NtNPR1	L52	NtNIMIN1-L	PL	edCer3Ndel2	0.98
ggSalicS_044	edAFPt9	SP	NtNPR1	L52	NtNIMIN1-L	PL	edCer3Ndel3	0.92
ggSalicS_045	edAFPt9	SP	NtNPR1	L52	NtNIMIN1-L	PL	edCer3Ndel6	0.95
ggSalicS_046	edAFPt9	SP	NtNPR1	L52	NtNIMIN1-L	PL	edCer3Ndel7	0.94
ggSalicS_047	edAFPt9	SP	NtNPR1	L52	NtNIMIN1-L	PL	edCer3Ndel8	0.92
ggSalicS_048	edAFPt9	SP	NtNPR1	L52	NtNIMIN1-L	PL	edCer3Ndel9	0.86
ggSalicS_049	edAFPt9	SP	NtNPR1	L52	NtNIMIN1-L	PL	WTCer3	1.00
ggSalicS_050	edAFPt9	SP	NtNPR1	L52	NtNIMIN1-L	PL	WTCer3Ndel1	0.97
ggSalicS_051	edAFPt9	SP	NtNPR1	L52	NtNIMIN1-L	PL	WTCer3Ndel2	0.98
ggSalicS_052	edAFPt9	SP	NtNPR1	L52	NtNIMIN1-L	PL	WTCer3Ndel3	0.98
ggSalicS_053	edAFPt9	SP	NtNPR1	L52	NtNIMIN1-L	PL	WTCer3Ndel5	0.98
ggSalicS_054	edAFPt9	SP	NtNPR1	L52	NtNIMIN1-L	PL	WTCer3Ndel6	0.97
ggSalicS_055	edAFPt9	SP	NtNPR1	L52	NtNIMIN1-L	PL	WTCer3Ndel7	0.95
ggSalicS_056	edAFPt9	SP	NtNPR1	L52	NtNIMIN1-L	PL	WTCer3Ndel8	0.96
ggSalicS_057	edAFPt9	SP	NtNPR1	L52	NtNIMIN1-L	PL	WTCer3Ndel9	0.96
ggSalicS_058	edAFPt9	SP	NtNPR1	L52	NtNIMIN1-L	PL	edTRQ2Ndel3	0.93
ggSalicS_059	edAFPt9	SP	NtNPR1	L52	NtNIMIN1-L	PL	edTRQ2Ndel4	0.95
ggSalicS_060	edAFPt9	SP	NtNPR1	L52	NtNIMIN1-L	PL	edTRQ2Ndel5	0.96
ggSalicS_061	edAFPt9	SP	NtNPR1	L52	NtNIMIN1-L	PL	edTRQ2Ndel6	0.95
ggSalicS_062	edAFPt9	SP	NtNPR1	L52	NtNIMIN1-L	PL	edTRQ2Ndel7	0.99

Table S4. Summary of SalicS1 candidates and their SA response. Description of each module and their linkers are summarized for all SalicS1 candidates with their emission ratio responding to 10 µM of SA *in vitro*.

Table S5.

Design		*In vitro*		*In vivo*		
NR		Kd	Maximum response	Transgenic lines	Brightness	Maximum response
NR1	R431K	N/A	N/A	No positive lines	N/A	N/A
NR2	R431A	N/A	N/A	No positive line	N/A	N/A
NR3	V432A	N/A	N/A	No positive line	N/A	N/A
NR4	R431Q	N/A	N/A	Yes	4096	0.005/0.008
NR5	A435F	N/A	N/A	Yes	2112	0.045
NR6	A435E	N/A	N/A	Yes	/	N/A
NR7	A446R	N/A	N/A	Yes	/	N/A
NR8	L515A	N/A	N/A	Yes	3285	0.12
HA						
HA1	S512Y	16.32	0.24	No positive lines	N/A	N/A
HA2	R422Q	9.942	0.24	Yes	/	/
HA3	K424R	1.584	0.15	Yes	4096	0.47/0.35
HA4	N430K	5.047	0.2	Yes	2816	0.22/0.21
HA5	L437F	11.84	0.23	Yes	/	/
HA6	Q441N	5.776	0.26	Yes	/	/
HA7	D443E	10.1	0.19	No positive lines	N/A	N/A
HA8	P459T	11.25	0.23	Yes	/	/
HA9	A446V	4.387	0.24	Yes	2816	0.36
LA						
LA1	T500A	39.97	0.23	No positive lines	N/A	N/A
LA2	V501A	20.26	0.16	Yes	/	/
LA3	F508A	36.17	0.15	Yes	3285	0.47/0.31

Table S5. Summary of SalicS1 and its variants SA response, expression and brightness. NR, non-responsive variants; HA, high-affinity variants; LA, low-affinity variants. Design of SalicS1 variants and their Kd and maximum response *in vitro* are presented. Transgenic lines were generated for these variants and summarized with their brightness and maximum response to SA.

Table S6.

	Independent lines generated	Pre-screen	Expression check	Good fluorescence	SA response check
nlsSalicS1	14 lines	14 lines	14 lines	5 lines	4 lines
NR					
NR1	No positive lines identified in T1				
NR2	No positive lines identified in T1				
NR3	No positive lines identified in T1				
NR4	6 lines	6 lines	3 lines	3 lines	2 lines
NR5	3 lines	3 lines	1 line	1 line	1 line
NR6	No positive lines identified in T1				
NR7	3 lines	3 lines	1 line	1 line	1 line
NR8	1 line	1 line	1 line	1 line	1 line
HA					
HA1	No positive lines identified in T1				
HA2	9 lines	9 lines	3 lines	2 lines	1 line
HA3	6 lines	6 lines	2 lines	2 lines	2 ines
HA4	2 lines	2 lines	2 lines	2 lines	2 lines
HA5	17 lines	17 lines	1 line	1 line	1 line
HA6	5 lines	5 lines	2 lines	2 lines	1 line
HA7	No positive lines identified in T1				
HA8	10 lines	10 lines	2 lines	2 lines	1 line
HA9	1 line	1 line	1 line	1 line	1 line
LA					
LA1	1 line	1 line	1 line	No line	1 line
LA2	10 lines	10 lines	10 lines	No line	No line
LA3	3 lines	3 lines	2 lines	2 lines	2 lines

Table S6. Summary of independent plant lines for each nlsSalicS1 variant. Independent plant lines generated, pre-screened, screened, and characterised were stated in the table.

Movie S1.
A surge of SA spreading from the *Pst* inoculation site at a cellular resolution reported by nlsSalicS1.

Data S1. (separate file)
Full description of all statistical tests performed in Main and supplementary figures.

Data S2. (separate file)
All primers used for cloning in this paper.